frontiers | Frontiers in Earth Science

TYPE Review
PUBLISHED 26 January 2023
DOI 10.3389/feart.2022.1109327

OPEN ACCESS

EDITED BY
Zhuang Li,
China University of Petroleum, China

REVIEWED BY
Chenguang Wang,
Hebei GEO University, China
Sam Uthup,
National Taiwan Normal University, Taiwan
Zhiwei Wang,
Hebei GEO University, China

*CORRESPONDENCE
Fei Xue,
fei.xue@hhu.edu.cn

SPECIALTY SECTION
This article was submitted to Petrology, a section of the journal Frontiers in Earth Science

RECEIVED 27 November 2022
ACCEPTED 07 December 2022
PUBLISHED 26 January 2023

CITATION
Xue F, Santosh M, Tsunogae T, Yang F, Tan H, Chen G, Li C and Xu Y (2023), Mesozoic magmatic evolution of the Laiyuan complex: Tracing the crust-mantle and lithosphere-asthenosphere interactions in the central North China Craton.
Front. Earth Sci. 10:1109327.
doi: 10.3389/feart.2022.1109327

Mesozoic magmatic evolution of the Laiyuan complex: Tracing the crust-mantle and lithosphere-asthenosphere interactions in the central North China Craton

Fei Xue[1]*, M. Santosh[2,3], Toshiaki Tsunogae[4], Fan Yang[5], Hongbing Tan[1], Guohui Chen[1], Chao Li[1] and Yunchou Xu[2]

[1]School of Earth Sciences and Engineering, Hohai University, Nanjing, China, [2]School of Earth Sciences and Resources, China University of Geosciences Beijing, Beijing, China, [3]Department of Earth Sciences, University of Adelaide, Adelaide, SA, Australia, [4]Graduate School of Life and Environmental Sciences, University of Tsukuba, Ibaraki, Japan, [5]Key Laboratory of Mineral Resources in Western China (Gansu Province), School of Earth Sciences, Lanzhou University, Lanzhou, China

The Laiyuan complex in the central North China Craton (NCC) incorporating different magmatic suites offers an excellent opportunity to investigate the lithospheric evolution and cratonic destruction. However, the petrogenesis and tectonic implications of this magmatic suite remain debated due to lack of integrated studies. Here we evaluate the magmatism and tectonic setting assembling data from multidisciplinary investigations of the Laiyuan complex. The complex is composed of volcanic suites, granitoids, ultramafic-mafic intrusions, and dykes showing common features of enrichments in LREEs and LILEs and depletions in HFSEs. Detailed petrogenetic considerations suggest that crust-mantle and lithosphere-asthenosphere interactions contributed to the formation of various magmatic suites. The involvement of thickened lower crust and enriched lithospheric mantle in the source, and diverse magmatic processes including partial melting, fractional crystallization, and magma mixing have played a significant role in the petrogenesis of the Laiyuan complex. Furthermore, the lithosphere-asthenosphere interaction induced by thinning lithosphere and upwelling asthenosphere controlled the source variations from dolerites to lamprophyres. The complex formed in an extensional tectonic setting triggered by the subduction of the Paleo-Pacific Plate. The subduction, rollback, and stagnation of the Paleo-Pacific slab contributed to the modification of the lithospheric architecture of the North China Craton. A slow and gradual thermal-mechanical erosion occurred at the central North China Craton whereas the rapid and intense lithospheric delamination occurred at the eastern North China Craton contributing to different lithospheric evolution. Both of the mechanisms combined with the subduction of Paleo-Pacific slab played a significant role in the destruction of the North China Craton and the formation of various magmatic suites. An integrated model is proposed to describe the magmatic evolution of the Laiyuan complex. During Jurassic, the subduction of the Paleo-Pacific Plate

reached beneath the central North China Craton. At 145–140 Ma, the fast slab rollback occurred and lead to hot asthenosphere upwelling and extensional setting in the central North China Craton inducing the crust-mantle interaction accounting for the petrogenesis for the formation of granitoids with MMEs (137–126 Ma), volcanic rocks (131–127 Ma), and felsic dykes (131–127 Ma). Through time, the lithosphere became substantially thin with the asthenospheric input increasing to form dolerite dykes at 125–117 Ma and lamprophyre dykes at 115–111 Ma.

KEYWORDS

North China Craton, Laiyuan complex, craton destruction, magmatic evolution, compositional diversity, crust-mantle interaction, lithosphere-asthenosphere interaction

1 Introduction

The cratonic roots are rigid, cold, and buoyant which could enable the overlying crust to resist extensive magmatism and crustal deformation except for minor eruptions of anorogenic and deep mantle-derived carbonatite, kimberlite, and related igneous rocks (e.g., Lee et al., 2011; Hawkesworth et al., 2017). However, the NCC shows distinct features of destruction after its formation. The NCC is one of the oldest cratons globally with a long evolutionary history during the Precambrian (Zhai and Santosh, 2011). Following its final cratonization during the late Paleoproterozoic, like other cratons, the NCC remained quiescent for a long time until the Mesozoic, when voluminous magmatism (e.g., Ma et al., 2014; Zhang et al., 2014; Dong et al., 2018; Zheng et al., 2018), associated metallogeny generated some of the world-class deposits (e.g., Groves and Santosh, 2016; Li and Santosh, 2017; Cai et al., 2018), and basin sedimentation (e.g., Li et al., 2012) occurred in the central and eastern NCC referred to as craton destruction or decratonization (e.g., Zhu et al., 2011). Detailed geological and geophysical studies have proved that more than 100 km of the ancient refractory lithospheric mantle has been eroded and replaced by young and fertile mantle materials beneath the eastern portion of the NCC since the Mesozoic (Gao et al., 2002; Liu X. et al., 2017; Liu et al., 2019; Wu et al., 2019).

The craton destruction of the NCC has been identified and studied in many previous pieces of research including the temporal-spatial distribution, mechanism, and geodynamic trigger (Fan, 1992; Griffin et al., 1998; Xu, 2001; Zheng et al., 2001; Gao et al., 2002; Wu et al., 2005; Menzies et al., 2007; Zhu et al., 2011; Zhang et al., 2014; Wu et al., 2017; Liu et al., 2019; Wu et al., 2019). Recent studies are paying more and more attention to the different lithospheric evolutions and destruction mechanisms in the eastern and central NCC. Continental delamination (Gao et al., 2004) and chemical-mechanical erosion (Xu, 2001) models have been used to interpret the intense magmatism and mineralization in the eastern NCC and its northern margins. However, the central NCC (craton interior) also witnessed extensive magmatism, especially in the Taihang Mountains (TM) forming diverse plutons or igneous complexes. Whether these magmatic suites were products of the craton destruction process and whether the lithosphere beneath the TM had a similar evolutional process with the lithosphere in the eastern NCC are still debated. As indicated by the geophysical data, the thickness of the lithosphere in the Jiaodong Peninsula is 60–100 km, whereas it is thicker (100–150 km thick) in the TM (Zhu et al., 2011; Liu et al., 2019). All these features suggest that the lithosphere beneath the central NCC has different lithospheric structures and lithospheric evolution from those of the eastern NCC. The northern Taihang Mountains (NTM) area is precisely also the border between the eastern and central NCC, marking the transitional zone of the two domains with different lithospheric evolutional processes and destruction mechanisms. Thus, by studying a magmatic complex from the NTM in the spatial-temporal-petrogenetic-tectonic aspects, the craton destruction and lithospheric evolution throughout the NCC could be well understood.

The processes associated with magmatism play important roles in the material differentiation of the Earth and the lithosphere (Rudnick, 1995). The course of magma from its source to ascent and emplacement usually involves several petrogenetic processes such as partial melting of the source, assimilation and fractional crystallization, and magma mixing and mingling, which eventually contribute to the formation of an igneous complex with compositional diversities (Annen et al., 2006; Spera and Bohrson, 2001). Igneous complexes or batholiths with variable rock types have attracted significant attention, providing critical petrological implications for petrogenesis, tectonic setting, crustal structure, and lithospheric evolution. In addition, the giant igneous complexes comprising various types of magmatic rocks are important targets to investigate the magmatic differentiation contributing to the compositional variations from mafic to felsic. In the North China Craton (NCC), during the Mesozoic, extensive magmatism occurred and formed lots of magmatic complexes offering the window to investigate the unique NCC destruction phenomenon.

To interpret the heterogeneity in the magmatic complex, several mechanisms have been proposed, such as aggregation of

multiple pulses of magma from partial melting, fractional crystallization of magma, magma mixing and mingling, assimilation and contamination of surrounding rocks, and liquid immiscibility (Zhu et al., 2012). Magma mixing, assimilation and contamination, and liquid immiscibility may be possible to generate stock-scale to enclave-scale intrusions but could not have the power to cause a pluton-scale intrusion with compositional variations (Wu et al., 2017). In contrast, partial melting and crystal fractionation are the main mechanisms devoted to the differentiation of granite (Gao et al., 2016). Partial melting means that the different portions of various types in the granitoid complex were directly crystallized from incremental batches of the magma (Glazner et al., 2004; Zak and Paterson, 2005; Walker Jr et al., 2007). When crystal fractionation dominates the formation of granites, different types of rocks were sourced from the same batch of magma by crystal separation and were crystallized in the magma chamber at different periods (Bateman and Chappell, 1979; Wilson, 1993; Pitcher, 1997). Therefore, the compositional characteristics of rocks generated by fractional crystallization do not necessarily equate to the source features, but it could reveal much physicochemical condition of the magma and its variation during crystallization (Xu et al., 2019). In the case of the Tuolumne magmatic complex in the Sierra Nevada, the origin of the composition variations of the variable magmatic suites has transformed from a traditional point of *in-situ* fractional crystallization (Bateman and Chappell, 1979) to prolonged partial melting of the sources at different periods (Coleman et al., 2004).

To sum up the above, the Laiyuan magmatic complex located at the central NCC which is composed of various magmatic rocks including mafic-ultramafic intrusive suites, intermediate-felsic intrusions, volcanic rocks, and dyke suites is selected as the perfect object to study the relationship between the magmatic evolution and compositional heterogeneity and to investigate the Mesozoic magmatism, lithospheric evolution, and lithospheric destruction in the NCC. Although there were many studies concentrated on magmatism and related mineralization in the TM (Chen et al., 2004; Chen et al., 2008; Chen et al., 2009; Zhang et al., 2011; Li et al., 2013; Zhang et al., 2015; Xue et al., 2019a; Li et al., 2019), the petrogenesis and tectonic setting of magmatic rocks in this area during Mesozoic are still debated. Some researchers favored the concept that the granitoids with adakitic affinity were formed by partial melting of the thickened mafic lower crust (Cai et al., 2003; He and Santosh, 2014; Zhang et al., 2016), whereas others highlighted the dominant role of fractional crystallization of magmas sourced from partial melting of the ancient enriched lithospheric mantle on the formation of variable magmatic suites (Gao et al., 2012; Hou et al., 2015; Li et al., 2019). In addition, the magma mixing and mingling process between mantle-derived basaltic magmas and siliceous crustal melts was also thought to be the possible petrogenesis for granitoids with adakitic features (Chen et al., 2013). Another remaining question is the relationship between the Mesozoic magmatism in the TM and the subduction of the Paleo-Pacific Plate: the direct impact (Chen et al., 2005) or the far-field effect (e.g., Yang et al., 2020) exerted by the slab subduction.

Thus, it is essential to study the magmatic complex on the whole, to conduct precise petrological studies on variable magmatic suites, and to reconstruct the evolutional process of the magmas according to the temporal series or lithologic sequence. Previous studies on the Laiyuan complex just focus on the single magmatic units and lack the concentrations on the genetic relationships between different magmatic units leading to the unilateral recognition of the magmatic evolution, petrogenesis, and tectonic setting. It should be noted that the formation of a voluminous complex with compositional variations cannot be generated by a single genesis, and it must involve multiple interactions among crust, lithospheric mantle, and/or asthenospheric mantle and various sources involved in the magma's evolution. In this review, based on multidisciplinary investigations carried out by us (Xue et al., 2019b; Xue et al., 2020; Xue et al., 2021) including field studies, petrology, mineral chemistry, whole-rock geochemistry, zircon U-Pb geochronology, zircon Hf isotopes, and geochemical modeling on different rock types from the Laiyuan complex, and previous literature, the objectives of this paper are (1) to clarify the rock types, mineral compositions, paragenetic order, and field relationship between various magmatic suites, (2) to constrain the geochronological framework of magmatism and investigate the geochronological implications on the NCC destruction, (3) to investigate the multiple sources and genesis of various rocks types and establish an integrated petrogenetic model for the Laiyuan complex, (4) to discuss the tectonic setting in the study area during Mesozoic and investigate the lithospheric evolution in the central NCC during Mesozoic.

2 Geological setting

2.1 North China craton

The North China Craton (NCC) is referred to as the oldest cratonic nuclei on Earth (Zhai and Santosh, 2011) and the main component of Chinese continental collage (Figure 1A) containing Eoarchean rocks as old as 3.8 Ga (Liu et al., 1992). With an area of ~1.5 million km^2, the NCC is sandwiched between the southwestern Qinling-Dabie Orogen, the southern Yangtze Craton, the southeastern Sulu Orogen, and the northern Central Asian Orogenic Belt (Figure 1A). The NCC has been divided into three major tectonic units (Zhao et al., 2005): the Western Block, the Eastern Block, and the Trans-North China Orogen (TNCO) (Figure 1A). It has a complex evolutional history from the amalgamation between the Eastern and Western blocks along the Trans-North China

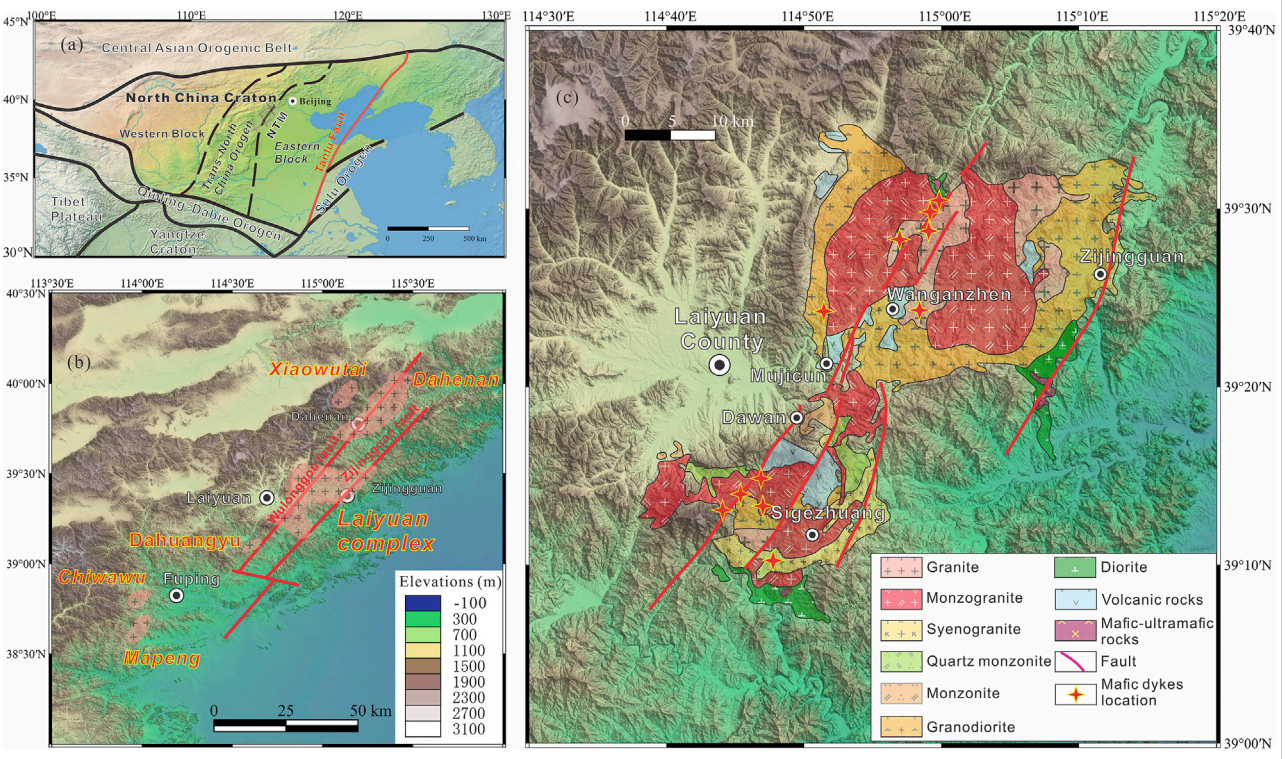

FIGURE 1
(A) Tectonic subdivision of the North China Craton (modified after Zhao et al., 2005). **(B)** Simplified geological map showing the distributions of Mesozoic intrusions in the NTM. **(C)** Geological map of the Laiyuan magmatic complex after the mineral and geological map in Laishui-Yixian areas (1979) and the locations of dyke suites.

Orogen at ~1.85 or 1.95 Ga (Zhai and Santosh, 2011; Zhao et al., 2012), to Mesozoic-Cenozoic destruction when extensive magmatism destroyed the cratonic architecture (e.g., Xue et al., 2021). The TNCO is a nearly north-south-trending orogen across the central part of the NCC. The basement rocks comprise Neoarchean to Paleoproterozoic tonalite-trondhjemite-granodiorite (TTG) gneisses, meta-supracrustal rocks, syn-to post-tectonic granitoids, mafic dykes, and ultramafic to mafic rocks. The present study area is located in the Fuping area in the NTM, along the eastern part of the TNCO (Figure 1A).

2.2 Northern Taihang Mountains

The TM is located at the boundary between the eastern and central NCC and marks the westernmost region of the Mesozoic magmatism with a length of ~700 km from the north to the south and a width of 50–100 km from the east to the west, connecting the southern Qinling-Dabie orogenic belt and northern Yanshan fold and thrust belt. The TM could be divided into two domains, the southern Taihang Mountains (STM) and the NTM (Figure 1B).

The major exposed strata in the area belong to the Archean basement metamorphic rocks, Proterozoic sedimentary sequences, Paleozoic sedimentary cover rocks, Mesozoic volcanic and volcaniclastic rocks, and Cenozoic sediments (Tang and Santosh, 2018). The Archean basement rocks are dominantly the Fuping Group represented by high-grade metamorphic rocks including TTG gneisses, amphibolite, marble, and magnetite-quartzite with metamorphic ages in the range of 2.5–2.7 Ga (Liu et al., 1984). These basement rocks are unconformably covered by Proterozoic sedimentary sequences. Unconformably covering the Paleoproterozoic sequences, the overlying Cambrian-Ordovician strata are dominantly composed of limestone (Dong et al., 2013). The Mesozoic strata are represented by a sequence of volcano-sedimentary rocks of andesite and andesitic breccia belonging to the Tiaojishan Formation, rhyolite, and rhyolitic breccia and tuff which have been dated as Jurassic to Cretaceous (Gao et al., 2012; Duan et al., 2016) unconformably underlying the Paleozoic sedimentary rocks. The above successions were intruded by extensive Mesozoic batholiths and stocks.

The NTM has experienced multiple tectonic activities including Archean EW trending folds, and Mesozoic NNE trending regional faults and folds. The EW axial trending

Fuping anticlinorium was developed in the Archean basement rocks with the metamorphic rocks of the Fuping Group in the core and Proterozoic to Paleozoic sedimentary rocks in the limbs. Furthermore, the Mesozoic folds show characteristics of NE-NEE axial trending and wide-shaped superimposed on the earlier Fuping folds. The major controlling structures in the NTM are the Mesozoic Zijingguan and Wulonggou faults (Figure 1B). These NNE-trending regional faults cut across the Precambrian basement and Paleozoic strata, and form part of the NE–SW-trending Daxin'anling–Taihangshan gravity lineament, considered as the lithospheric boundary between the TNCO and the Eastern Block (Niu, 2005). The NEE-trending framework controls the distribution of large plutons and extrusive rocks in this area (Figure 1B).

As discussed above, the TM witnessed extensive magmatism occurred since the late Mesozoic, generating voluminous eruption of intermediate-felsic volcanic rocks, and large granitoid batholiths and plutons which are distributed in the NTM and the STM (Figure 1B). The NTM hosts plutons and stocks including the Yunwushan, Dahaituo, Sihai, Dahenan, Wanganzhen and Sigezhuang (Laiyuan magmatic complex), Chiwawu, and Mapeng plutons (Figure 1B). The intrusive rocks in the NTM are characterized by intermediate-felsic granitic rocks represented by monzogranite, syenogranite, quartz monzonite, and monzonite (Li et al., 2013; He and Santosh, 2014; Zhang et al., 2016; Yang et al., 2019a). In the NTM, the Laiyuan magmatic complex comprising the Wanganzhen and Sigezhuang plutons (Figure 1C) is the most representative intrusion which incorporates several magmatic suites consisting of voluminous granitoid plutons, sporadic extrusive volcanic lava, small ultramafic-mafic intrusive bodies, and mafic-felsic dykes. The detailed discussion about the petrology of this complex and the geochronological framework of the magmatic rocks in the NTM will be discussed in the following sections.

3 Petrographic characteristics of the Laiyuan magmatic complex

The Laiyuan complex is the largest volcano-plutonic complex in the NTM with a NEE-trending dumbbell shape and a total outcrop area of over 1,000 km^2 (Figure 1C). The complex has been divided into two domains: the northern Wanganzhen pluton and the southern Sigezhuan pluton with a multi-stage magmatic history of at least three distinct phases (Cai et al., 2003) leading to multiple ringed structures from the periphery to the core (Figure 1C). The Laiyuan magmatic complex is composed of ultramafic-mafic rocks, granitoids, eruptive rocks, and tiny dyke suites. Integrated fieldwork was conducted in the Laiyuan complex with a collection of representative samples from different magmatic suites (Xue et al., 2019b; Xue et al., 2020; Xue et al., 2021).

3.1 Volcanic rocks

The volcanic rocks cover Paleozoic Cambrian-Ordovician strata. Based on petrological features, they belong to the andesite-dacite-rhyolite series (Figures 2A–C). The andesites are characterized by porphyritic texture with plagioclase, amphibole, and pyroxene occurring as phenocrysts accounting for ~40% (Figure 3A). The matrix is characterized by a typical pilotaxitic texture with oriented plagioclase microcrystals accounting for ~60% (Figure 3A). The dacites have plagioclase, K-feldspar, clinopyroxene, and amphibole occur as phenocrysts accounting for ~35% (Figure 3B). The rhyolite is characterized by grey greenish color and is composed of quartz, plagioclase, biotite, and amphibole phenocrysts (Figure 3C). Plagioclase, K-feldspar, and quartz constitute the matrix with magnetite, apatite, and zircon as the accessory minerals.

3.2 Granitoids

The granitoids account for the major domain of the Laiyuan complex incorporating variable lithologies. In the field, the contact between different magmatic units is sometimes clear indicating they emplaced in multiple magmatic events, not crystallized from single magmatism (Figure 2D). A particular feature of the Laiyuan magmatic complex is that abundant enclaves and xenoliths (Precambrian felsic gneisses fragments) are founded in this huge granitic batholith (Figures 2E–H). The felsic and mafic dykes intruded the granitoids in some regions of the complex exhibiting a clear contact relationship with the host granitoids (Figures 2I, M).

The major rock types are syenogranite, monzogranite (porphyritic monzogranite), quartz monzonite, and monzonite (Figures 2D–H). The syenogranites are exposed along the rim of the pluton and exhibit massive structure and flesh-red color (Figure 2F). They are coarse to medium-grained and show typical granitic texture with abundant K-feldspar minerals (Figure 3D). They are composed of microcline (~50%) or K-feldspar (~45–50%), quartz (~30%), plagioclase (15%–20%), and biotite (~5%). The monzogranite occupies major domains and is exposed in the core of the intrusive complex and majorly comprises K-feldspar (~30–35%), plagioclase (~25–30%), quartz (~25–35%), biotite (~5–10%), hornblende (~3–5%), and some accessory minerals including magnetite, sphene, and zircon. Rapakivi texture (Figure 3E) and porphyritic texture (Figure 3F) also occurred in the monzogranite rocks containing abundant mafic microgranular enclaves (MMEs). The quartz monzonites are grey-white or grey-colored, medium-grained, and display massive structure and monzonitic texture. Euhedral to subhedral plagioclase (~25–35%), euhedral K-feldspar (~30–35%), anhedral quartz (~15–20%), euhedral biotite (~10–20%), and euhedral to subhedral hornblende (~10–20%) account for the mineral phases of the quartz monzonites. The zoning texture is common in plagioclase (0.6–2.0 mm) and K-feldspar (0.5–3.0 mm) crystals (Figures 3G, H).

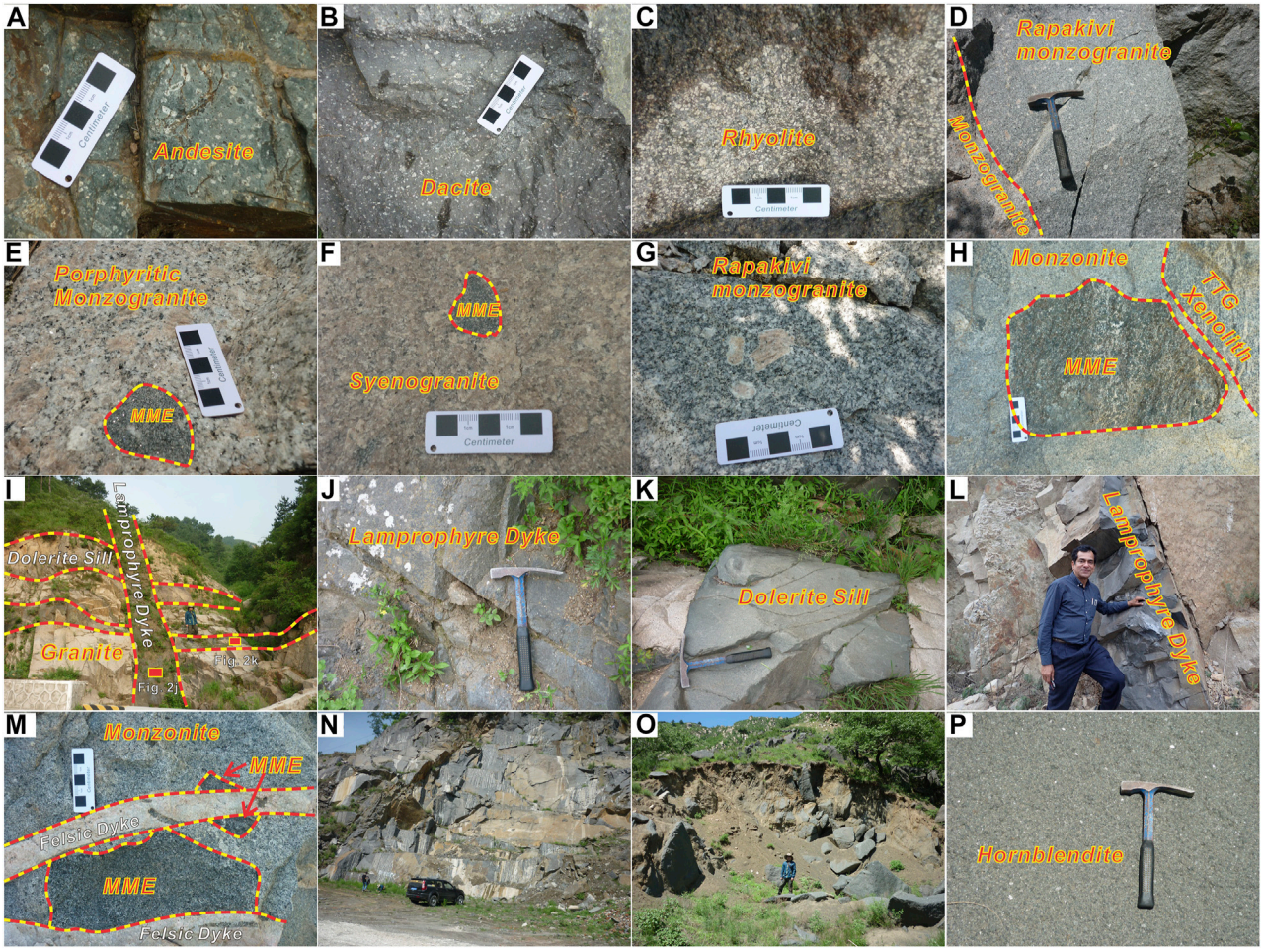

FIGURE 2
(A–C) The exposures of volcanic rocks in the field. **(D)** Contact zone between rapakivi monzogranite and porphyritic monzogranite. **(E)** Porphyritic monzogranite containing MME. **(F)** Pinkish syenogranite containing MME. **(G)** Rapakivi texture in monzogranite. **(H)** Monzonite containing mafic xenolith and TTG fragments from basement rocks. **(I)** Dolerite sills cut by later vertical lamprophyre dyke **(J)** Greyish green colored lamprophyre with abundant mafic phenocrysts **(K)** Dolerite sill showing compositional variations from margin to core **(L)** Fine-grained and dark gray colored lamprophyre dyke intruding host granite **(M)** Monzonite containing MME cut by later felsic dyke **(N,O)** Exposures of Longmengou pyroxenite and Yaogou hornblendite **(P)** Medium-grained hornblendite from Yaogou.

The monzonite and monzonite porphyry were at the northern and western rim of the pluton and are composed of plagioclase (~35–40%), K-feldspar (~30–35%), hornblende (~5–15%), biotite (~5–20%), and quartz (~5%). The zoning texture is identified in euhedral plagioclase grains, with a size of 0.1–2.0 mm, which were sometimes included in K-feldspar grains (Figure 3I).

3.3 Dyke suites

Abundant mafic dykes were identified in the Laiyuan area intruding the granitoids, Archean gneisses, and Paleozoic dolomites. The dykes intrude host granitoids and show sharp contact with the surrounding rocks suggesting rapid ascent of magma and fast solidification (Figures 2I, L). The lamprophyre dykes are generally fine-grained with typical lamprophyric texture of abundant mafic minerals occurring as phenocrysts (Figure 2J). The phenocryst phases are dominantly composed of euhedral to subhedral mafic minerals of amphibole, clinopyroxene, biotite (phlogopite), and minor olivine dominantly (40%–50%; by volume) which are at some places altered to carbonate, chlorite, and sericite (Figures 3J, K). The matrix is composed of pyroxene, hornblende, and plagioclase crystallites (Figure 3). The dolerite dykes are gray to light green and display massive structure (Figure 2K). They are composed of euhedral to subhedral plagioclase (~50%), subhedral altered pyroxene (~35%), stumpy biotite crystallite (~10%), and altered mineral of calcite (~10%) with accessory mineral of zircon. Besides mafic dykes, felsic dykes are also widespread in the Laiyuan complex (Figure 3L).

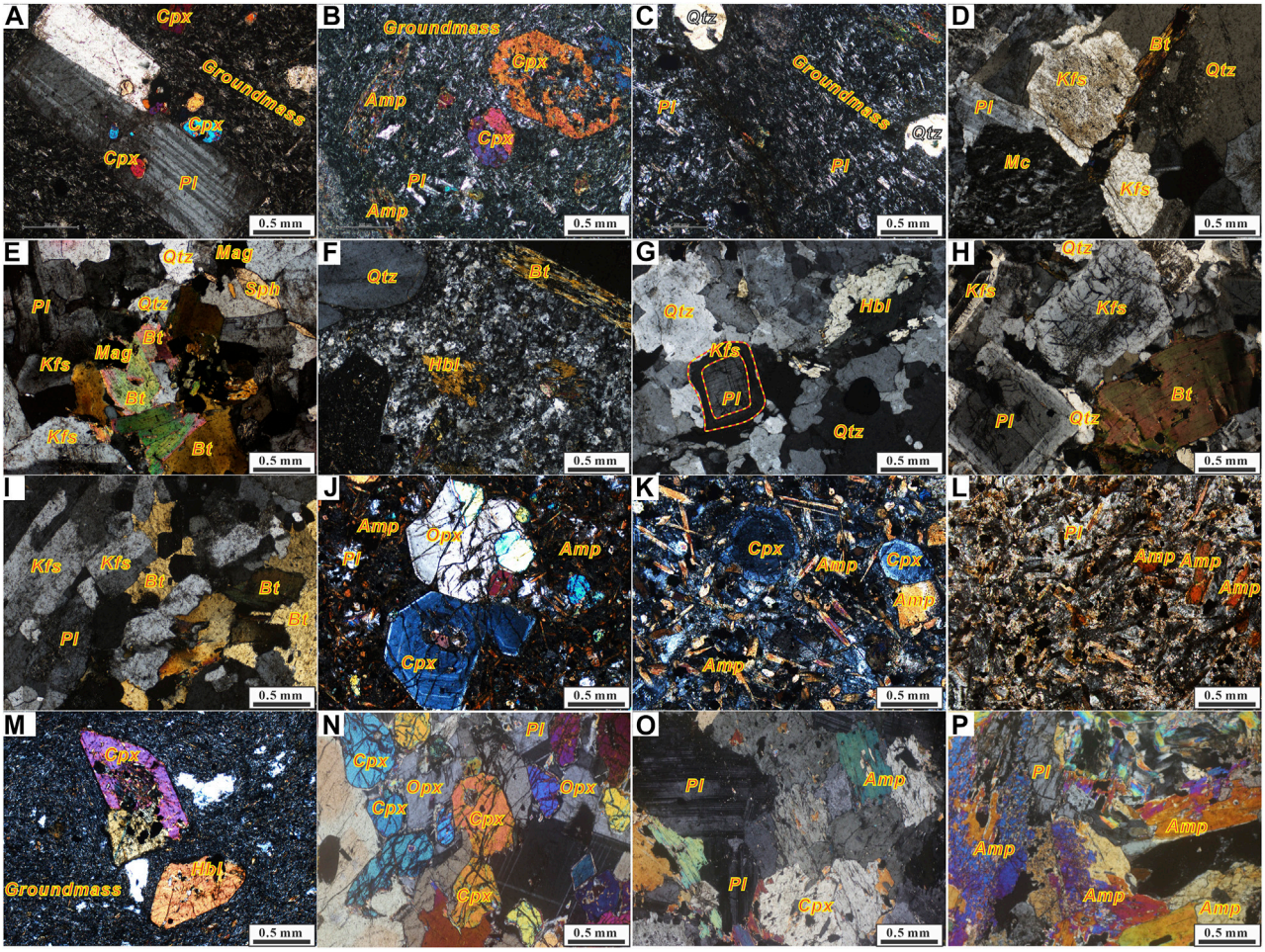

FIGURE 3
Representative photomicrographs of the Laiyuan magmatic rocks. **(A–C)** Andesite, dacite and rhyolite from the Laiyuan complex. **(D)** Syenogranite. **(E)** Biotite monzogranite. **(F)** Porphyritic monzogranite. **(G)** Rapakivi hornblende monzogranite. **(H)** Quartz monzonite showing zoning K-feldspar and plagioclase. **(I)** Monzonite **(J,K)** Lamprophyre containing clinopyroxene and orthopyroxene minerals of zoning texture and strip amphibole minerals **(L)** Dolerite **(M)** Diorite porphyry containing clinopyroxene and hornblende phenocrysts **(N,O)** Pyroxenite and gabbro from the Longmengou intrusions **(P)** Hornblendite from the Yaogou intrusions. Mineral abbreviations: Amp-amphibole; Ap-apatite; Bt-biotite; Cpx-clinopyroxene; Cal-calcite; Hbl-hornblende; Kfs-K-feldspar; Mag-magnetite; Mc-Microcline; Ol-olivine; Opx-Orthopyroxene; Pl-plagioclase; Qtz-quartz; Sph-sphene.

They are exhibiting porphyritic texture with matrix and phenocryst occupying 80% and 20%, respectively (Figure 3M). The phenocrysts consist of euhedral-subhedral hornblende (~10%), xenomorphic plagioclase with corrosion border (~5%), xenomorphic and tabular biotite (~5%), and quartz (~2%). The matrix contains abundant rhombic hornblende microlites ranging from 20 to 300 μm (35%), very fine-grained feldspar (~25%), and some other cryptocrystalline minerals (~15%).

3.4 Ultramafic-mafic rocks

Except for the collected volcanic rocks, granitoids, and dyke suites, the ultramafic-mafic rocks were outcropped in some places of the complex, such as Yaogou and Longmengou which have been studied by several researches (Liu et al., 2009; Liu et al., 2010; Gao et al., 2012; Zhai et al., 2014; Hou et al., 2015; Zhang et al., 2017). At Longmengou (Figure 2N; Figure 3N, O), the ultramafic-mafic rocks consist mainly of three rock units: hornblende pyroxenite, hornblende gabbro, and gabbroic diorite (Liu et al., 2010). The pyroxenite unit shows typical cumulate textures. The Yaogou ultramafic-mafic rocks are dominated by pyroxene hornblendite and gabbronorite (Figure 2O, P; Figure 3P), and occur as isolated bodies in the rim of the Wanganzhen pluton (Figure 1C). The hornblendite bodies at Yaogou occur as variously sized enclaves or rock blocks scattered in the gabbronorite intrusion (Hou et al., 2015). These ultramafic-mafic rocks are commonly hosted in granitoids including diorite and quartz diorite.

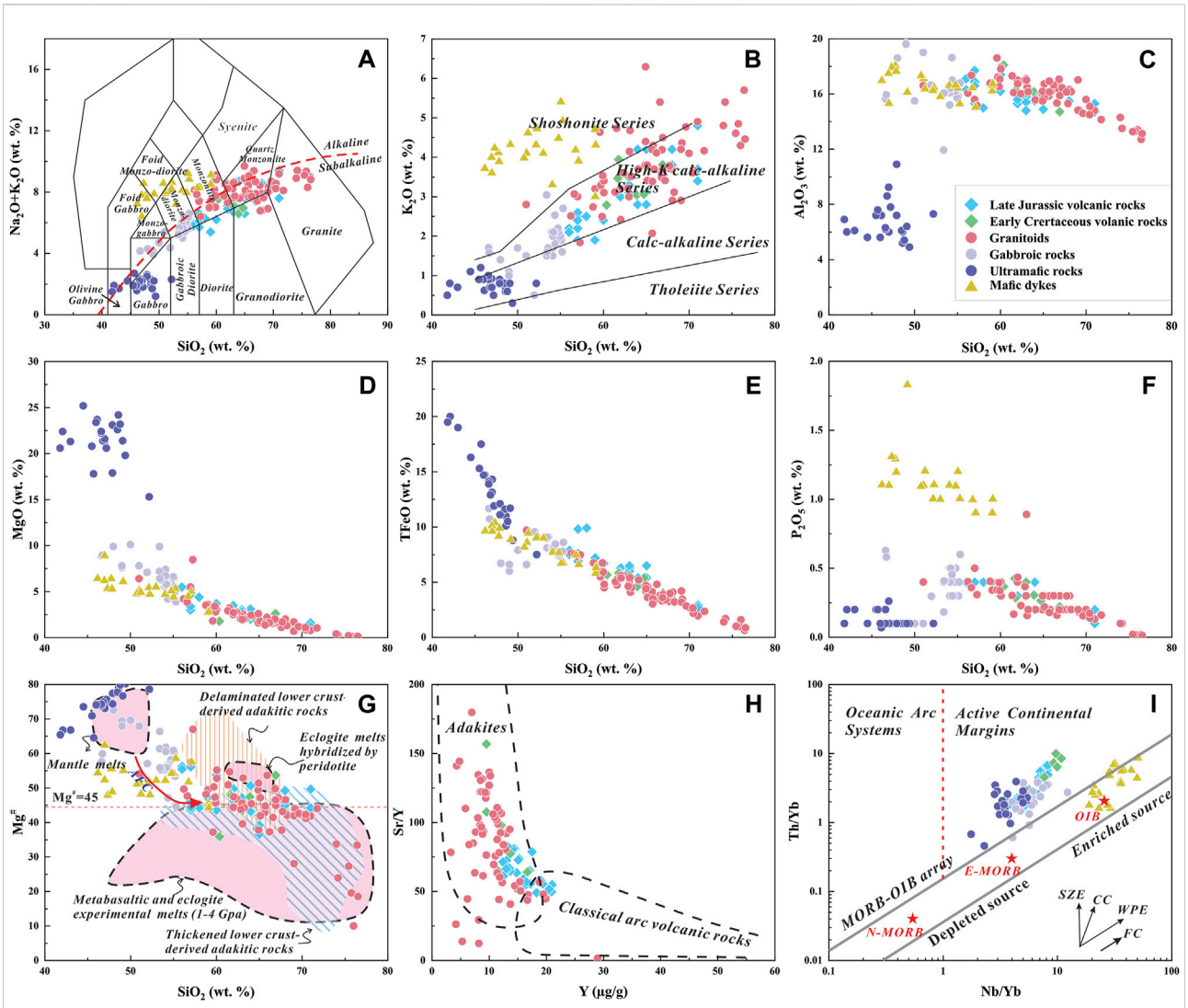

FIGURE 4
(A) TAS diagram for Laiyuan magmatic rocks (Middlemost, 1994). **(B)** K_2O vs SiO_2 classification diagram (Peccerillo and Taylor, 1975). **(C–F)** Selected major elemental variation diagrams for the Laiyuan magmatic rocks. **(G)** $Mg^{\#}$ vs SiO_2 (wt%) diagram. AFC curve is modified after (Stern and Kilian, 1996). Fields of metabasaltic and eclogite experimental melts hybridized with peridotite are after (Rapp et al., 1999). Field of metabasaltic and eclogitic melts (1–4 GPa) is after (Wang et al., 2006) and (Rapp and Watson, 1995). Fields of delaminated and thick lower crust-derived adakitic rocks are after (Wang et al., 2006). **(H)** Sr/Y vs Y diagram. Fields of adakites and classical island andesite–dacite–rhyolite rocks are modified from Defant and Drummond (1990). **(I)** Th/Yb vs Nb/Yb diagram (after Pearce, 2008). Data source: Chang et al., 2021; Chen et al., 2003; Chen and Zhai, 2003; Gao et al., 2012; Gao et al., 2013; Hou et al., 2015; Liu et al., 2010; Qu, 2012; Xue et al., 2019b; Xue et al., 2020; Xue et al., 2021.

3.5 Spatial links between diverse magmatic suites

The volcanic series of andesites and dacites are exposed in horizontal integration of contact relationships (Figure 2A) indicating they were formed by the same volcanism. In terms of volume, the granitoids occupy most of the Laiyuan complex and occur as the host rocks for ultramafic-mafic suites in the borders of the complex (Figure 1C). The mafic rocks were hosted by the granitoids in the forms of small enclaves or large stocks indicating the emplacement of granitoids was slightly later than or simultaneous with the mafic intrusions (Figure 2H). The concentrically-zoned granitoids comprise diverse magmatic units. Contact boundaries between these various intrusive suites are legible and clear (Figure 2D) which are called pulsating contact relationships indicating they were formed simultaneously. As well, the containing MMEs in the granitoids have clear contact boundaries suggesting their similar formation ages (Figures 2E, F). Furthermore, the felsic dykes intruded the granitoids and cut the MMEs (Figure 2M), and diverse mafic dykes were identified in the granitoids throughout the complex (Figure 1C). The dolerite sills were cut by the vertical lamprophyre dykes exhibiting the

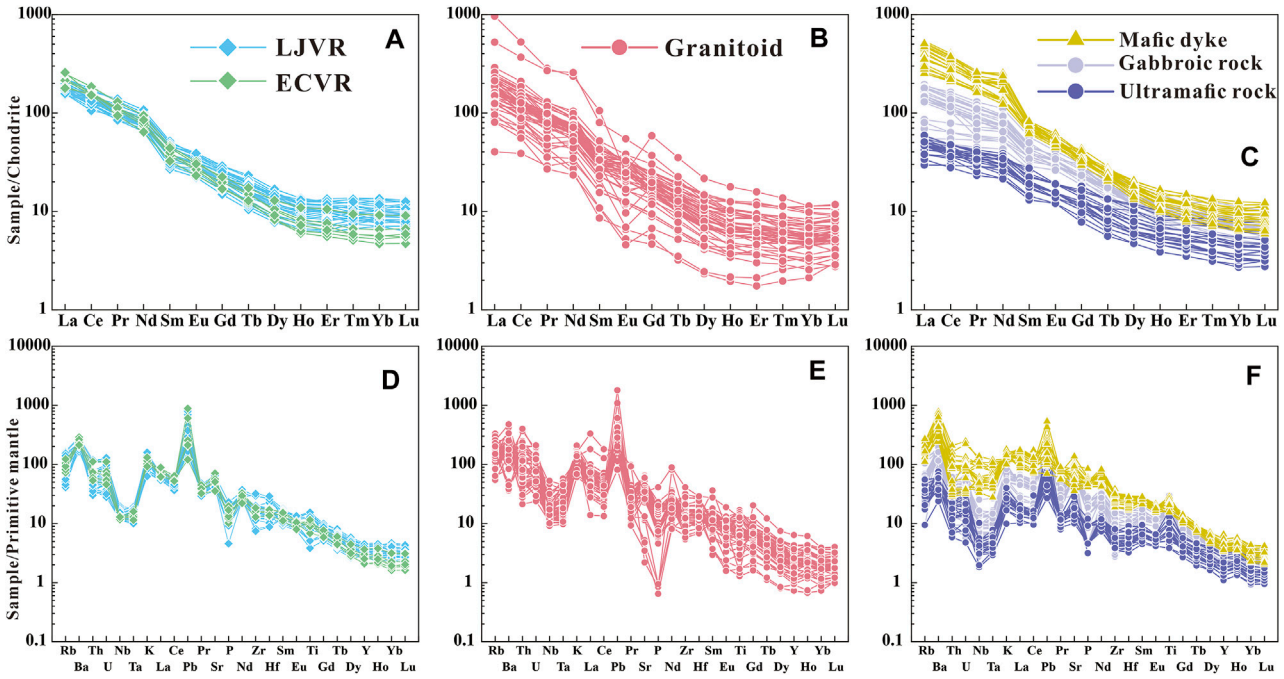

FIGURE 5
(A–C) Chondrite-normalized REE patterns for the Laiyuan magmatic rocks. **(D–F)** Primitive mantle-normalized trace element diagrams for of the Laiyuan magmatic rocks. Normalized values: chondrite (Mcdonough and Sun, 1995), primitive mantle (Sun and Mcdonough, 1989). Data source are same as in Figure 4.

lamprophyre dyking event as the latest magmatism in the Laiyuan complex (Figure 2I).

4 Geochemical features of the Laiyuan magmatic complex

Based on the analytical results of our studies (Xue et al., 2019b; Xue et al., 2020; Xue et al., 2021), the geochemical features are summarized. The Laiyuan volcanic rocks all show intermediate to felsic geochemical features and are classified as trachyandesite, andesite, trachydacite, and dacite in TAS diagram, and belong to high-K calc-alkaline series (Figures 4A, B). In the chondrite-normalized REE patterns (Figure 5A), the volcanic rocks are all enriched in LREEs relative to HREEs without significant Eu anomalies. As shown in the primitive mantle-normalized spidergram (Figure 5D), the Laiyuan volcanic rocks all show similar characteristics of enrichment in large ion lithophile elements (LILEs; e.g., Ba and Pb), and strong depletion in high field strength elements (HFSEs; e.g., Ti and Ta-Nb). The Laiyuan granitoids exhibit variations in their rock type including syenogranite, monzogranite, quartz monzonite, monzonite and granodiorite, and mostly belong to the high-K calc-alkaline series (Figures 4A, B). They are also characterized by metaluminous to weakly peraluminous features (Xue et al., 2021). Chondrite-normalized REE patterns for the Laiyuan granitoids are strongly fractionated with high $(La/Yb)_N$ and LREE/HREE ratios (Figure 5B). The syenogranite samples show strongly negative Eu anomalies different from other granitoids with almost no Eu anomalies (Figure 5B). In primitive mantle normalized spider diagram, these granitoids are enriched in LILEs and are distinctively depleted in HFSEs similar to the volcanic rocks (Figure 5E). Furthermore, the volcanic rocks and granitoids show similar adakitic features (Figure 4H).

According to the study by Chang et al. (2021), the mafic rocks in the Laiyuan complex are mainly hornblendites, pyroxenites, and gabbros. The ultramafic rocks show features of cumulative rocks which are characterized by high contents of MgO, TFeO and MnO but very low contents of SiO_2, Al_2O_3, Na_2O and K_2O (Figures 4A–G). They are all characterized by enrichment in LREEs and LILEs and depletion in HFSEs (Figures 5C, F). In addition, the gabbros are similar to the mafic dykes showing low concentrations of SiO_2 and high contents of MgO. The lamprophyres also show shoshonitic characteristics (Figures 4A, B), and belong to the alkali lamprophyre. Compared with lamprophyres, the dolerite dykes display a broad compositional change. Their SiO_2 and MgO contents are lower than those of lamprophyres but they also have shoshonitic features similar to lamprophyres. Furthermore, the felsic dykes show similar geochemical features to granitoids indicating their genetic relationship. In chondrite-normalized REEs

TABLE 1 Compilation of age data of the Laiyuan magmatic rocks.

No.	Locations	Rock types	Ages	2σ	Methods	References
1	Wanganzhen pluton	Andesite	145.3	0.4	LA-ICP-MS Zircon U-Pb	Duan et al. (2016)
2	Wanganzhen pluton	Andesite	144.6	0.8	LA-ICP-MS Zircon U-Pb	Duan et al. (2016)
3	Wanganzhen pluton	Andesite	145.6	4.7	LA-ICP-MS Zircon U-Pb	Gao et al. (2012)
4	Mujicun	Diorite porphyry	144.1	1.2	LA-ICP-MS Zircon U-Pb	Dong et al. (2013)
5	Mujicun	Diorite porphyry	141.7	1.6	LA-ICP-MS Zircon U-Pb	Gao et al. (2011)
6	Mujicun	Diorite porphyry	142.7	1.6	LA-ICP-MS Zircon U-Pb	Gao et al. (2002)
7	Dawan	Rhyolite porphyry	139.7	6.2	Whole-rock Rb-Sr	Hou et al. (2015)
8	Dawan	Rhyolite porphyry	141.2	0.7	LA-ICP-MS Zircon U-Pb	Song et al. (2014)
9	Sigezhuang pluton	Andesite-dacite	131.4	0.9	LA-ICP-MS Zircon U-Pb	Xue et al. (2020)
10	Sigezhuang pluton	Andesite-dacite	130.3	0.8	LA-ICP-MS Zircon U-Pb	Xue et al. (2020)
11	Sigezhuang pluton	Andesite-dacite	127.1	1.3	LA-ICP-MS Zircon U-Pb	Xue et al. (2020)
12	Longmengou	Hornblendite	154.2	4.5	Hbl Ar-Ar	Hou et al. (2015)
13	Longmengou	Hornblendite	132.5	2.1	Hbl Ar-Ar	Hou et al. (2015)
14	Longmengou	Gabbro	133.5	1.4	LA-ICP-MS Zircon U-Pb	Chang et al. (2021)
15	Longmengou	Gabbro	138.0	2.0	SHRIMP Zircon U-Pb	Chen et al. (2005)
16	Longmengou	Hornblende gabbro	139.7	2.6	LA-ICP-MS Zircon U-Pb	Zhang, (2014)
17	Sigezhuang pluton	MME	126.1	2.5	SHRIMP Zircon U-Pb	Chen et al. (2007)
18	Sigezhuang pluton	MME	128.7	2.1	SHRIMP Zircon U-Pb	Chen et al. (2009)
19	Sigezhuang pluton	MME	127.9	2.1	SHRIMP Zircon U-Pb	Chen et al. (2009)
20	Laiyuan complex	Diorite	135.6	2.6	LA-ICP-MS Zircon U-Pb	Chang et al. (2021)
21	Laiyuan complex	Diorite	128.5	2.2	LA-ICP-MS Zircon U-Pb	Chang et al. (2021)
22	Laiyuan complex	Diorite	135.0	3.0	LA-ICP-MS Zircon U-Pb	Chang et al. (2021)
23	Laiyuan complex	Aplite	132.7	1.8	LA-ICP-MS Zircon U-Pb	Chang et al. (2021)
24	Sigezhuang pluton	Quartz monzonite	132.0	2.0	SHRIMP Zircon U-Pb	Chen et al. (2005)
25	Wanganzhen pluton	Monzonite	129.0	2.6	SHRIMP Zircon U-Pb	Chen et al. (2005)
26	Wanganzhen pluton	Monzonite	133.3	3.0	LA-ICP-MS Zircon U-Pb	Qu, (2012)
27	Wanganzhen pluton	Granodiorite	135.7	1.3	SHRIMP Zircon U-Pb	Shen et al. (2015a)
28	Wanganzhen pluton	Monzogranite	133.7	1.1	SHRIMP Zircon U-Pb	Shen et al. (2015b)
29	Sigezhuang pluton	Syenogranite	133.1	0.5	LA-ICP-MS Zircon U-Pb	Xue et al. (2021)
30	Sigezhuang pluton	Monzonite	131.9	0.9	LA-ICP-MS Zircon U-Pb	Xue et al. (2021)
31	Sigezhuang pluton	Syenogranite	129.9	1.0	LA-ICP-MS Zircon U-Pb	Xue et al. (2021)
32	Sigezhuang pluton	Monzogranite	128.2	0.7	LA-ICP-MS Zircon U-Pb	Xue et al. (2021)
33	Sigezhuang pluton	Quartz monzonite	127.9	0.6	LA-ICP-MS Zircon U-Pb	Xue et al. (2021)
34	Zhijiazhuang	Granite	134.2	0.3	LA-ICP-MS Zircon U-Pb	Yang et al. (2019a)
35	Zhijiazhuang	Dioritic porphyry	129.0	0.6	LA-ICP-MS Zircon U-Pb	Yang et al. (2019b)
36	Zhijiazhuang	Monzonite	129.5	0.4	LA-ICP-MS Zircon U-Pb	Yang et al. (2019a)

(Continued on following page)

TABLE 1 (*Continued*) Compilation of age data of the Laiyuan magmatic rocks.

No.	Locations	Rock types	Ages	2σ	Methods	References
37	Wanganzhen pluton	Granodiorite	128.3	1.9	LA-ICP-MS Zircon U-Pb	Zhang, (2014)
38	Wanganzhen pluton	Monzogranite	129.8	2.7	LA-ICP-MS Zircon U-Pb	Zhang, (2014)
39	Wanganzhen pluton	Granodiorite	129.0	2.7	LA-ICP-MS Zircon U-Pb	Zhang et al. (2016)
40	Wanganzhen pluton	Quartz diorite	128.3	1.9	LA-ICP-MS Zircon U-Pb	Zhang et al. (2016)
41	Laiyuan complex	Felsic dyke	130.6	1.0	LA-ICP-MS Zircon U-Pb	Chang et al. (2021)
42	Laiyuan complex	Felsic dyke	126.9	0.8	LA-ICP-MS Zircon U-Pb	Xue et al. (2019b)
43	Laiyuan complex	Dolerite	125.2	1.0	LA-ICP-MS Zircon U-Pb	Xue et al. (2019b)
44	Laiyuan complex	Dolerite	123.5	0.9	LA-ICP-MS Zircon U-Pb	Xue et al. (2019b)
45	Laiyuan complex	Dolerite	122.5	1.2	LA-ICP-MS Zircon U-Pb	Xue et al. (2019b)
46	Laiyuan complex	Dolerite	120.2	0.8	LA-ICP-MS Zircon U-Pb	Xue et al. (2019b)
47	Laiyuan complex	Dolerite	116.6	0.7	LA-ICP-MS Zircon U-Pb	Xue et al. (2019b)
48	Laiyuan complex	Lamprophyre	114.2	4.1	LA-ICP-MS apatite U-Pb	Chang et al. (2021)
49	Laiyuan complex	Lamprophyre	114.5	1.0	LA-ICP-MS Zircon U-Pb	Xue et al. (2019b)
50	Laiyuan complex	Lamprophyre	112.8	1.3	LA-ICP-MS Zircon U-Pb	Xue et al. (2019b)
52	Laiyuan complex	Lamprophyre	112.2	0.9	LA-ICP-MS Zircon U-Pb	Xue et al. (2019b)
52	Laiyuan complex	Lamprophyre	111.0	1.2	LA-ICP-MS Zircon U-Pb	Xue et al. (2019b)

patterns (Figures 5C, F), all of the mafic rocks show features of enrichment in LREEs and the lack of obvious Eu anomalies. In the primitive mantle-normalized spidergram (Figure 5F), they show enrichment in fluid-mobile LILEs. The dolerites show strong depletion in HFSEs, but Th-U and Ta-Nb depletions in lamprophyres are not obvious, implying the different sources of dolerites and lamprophyres.

Additionally, besides the cumulative ultramafic rocks, the other rocks defined a continuous variation trend from the mafic rocks to granitoids in the Harker diagram indicating the tight genetic relationship between diverse magmatic suites (e.g., MgO -SiO_2 diagram, Figures 4C–F). The Laiyuan magmatic rocks are also showing common features of enrichments in LREEs and LILEs and depletions in HFSEs suggesting the significant role of lithospheric mantle in the genesis of the Laiyuan magmatic complex (Figures 5A–F).

5 Petrogenetic evolution of the Laiyuan magmatic complex

5.1 Temporal evolution of the Laiyuan magmatic suites

Several geochronological studies have been conducted in the Laiyuan complex focusing on the ultramafic-mafic rocks (Chen et al., 2005; Zhang, 2014; Hou et al., 2015; Chang et al., 2021), intermediate-felsic granitoids (Chen et al., 2005; Chen et al., 2007; Chen et al., 2009; Qu, 2012; Zhang, 2014; Zhang et al., 2016), volcanic and sub-volcanic rocks (Gao et al., 2011; Gao et al., 2012; Gao et al., 2013; Dong et al., 2013; Song et al., 2014; Duan et al., 2016), and mafic-felsic dyke suites (Xue et al., 2019b; Chang et al., 2021). By combining available dating results yielded from this study and literature (Table 1), the temporal connection between diverse magmatic suites could be established (Figure 6A).

The ultramafic-mafic rocks are majorly exposed in Longmengou and Yaogou areas with lithology dominated by hornblendite, pyroxenite, gabbro, and gabbroic diorite occurring as isolated bodies around the complex (Liu et al., 2009; Liu et al., 2010; Zhai et al., 2014; Zhang et al., 2017). Hou et al. (2015) yielded hornblende ^{40}Ar-^{39}Ar ages of 154 and 133 Ma from the Yaogou hornblendite, and Chen et al. (2005), Zhang (2014) and Chang et al. (2021) dated the Longmengou gabbro and gabbroic diorite at 140–134 Ma, respectively. The field and petrographical investigations indicate that these ultramafic-mafic bodies resulted from independent magmatic events, rather than xenoliths captured by the surrounding granitoids (Zhai et al., 2014; Zhang et al., 2017). As indicated by the spatial and temporal relationships, the ultramafic-mafic rocks act as the earliest intrusive phases of the magmatic evolutional series in the Laiyuan complex ranging from Late Jurassic to Early Cretaceous (154–133 Ma).

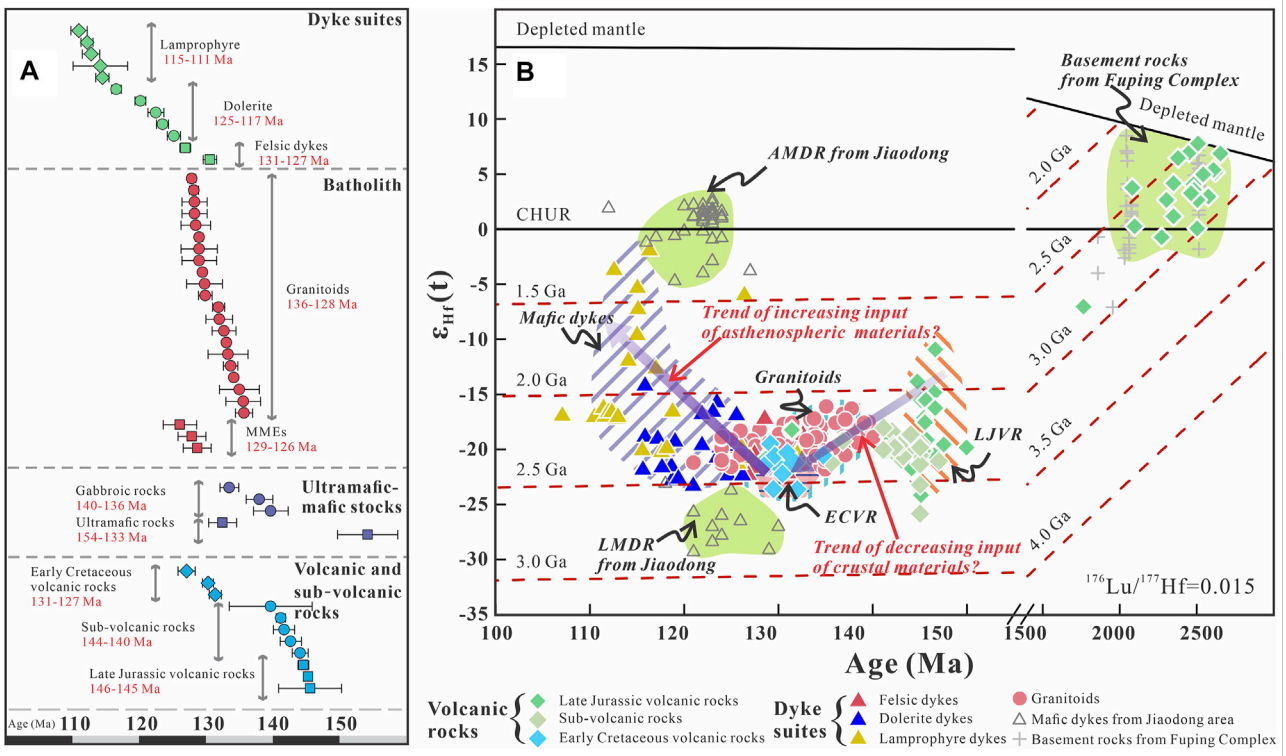

FIGURE 6
(A) Compilation of age data on the Laiyuan magmatic rocks. See Table 1 for data source. **(B)** Zircon $\varepsilon_{Hf}(t)$ values vs age diagram for the Laiyuan magmatic rocks. Data source: Basemen rocks of the Fuping Complex (Tang et al., 2015; Tang et al., 2016); Granitoids from the Laiyuan complex (Shen et al., 2015a; Yang et al., 2019b; Xue et al., 2021); Late Jurassic volcanic rocks (Duan et al., 2016); Sub-volcanic rocks (Qu, 2012; Shen et al., 2015b); Early Cretaceous volcanic rocks (Xue et al., 2021); Dyke suites from the Laiyuan complex (Xue et al., 2019b) and Shandong Peninsula (Ma et al., 2014; Ma et al., 2016).

The earliest intrusive phases were followed by Late Jurassic volcanic episodes (146–145 Ma, Figure 6A) in some places within the complex. This volcanic episode was characterized by andesitic-dacitic-rhyolitic lava eruption accounting for the typical Mujicun caldera which is composed of welded breccias, ignimbrite sheets, and lava flows (Gao et al., 2012). Within the volcanic edifice, a half ring of small sub-volcanic stocks and plugs associated with porphyry Cu-Mo deposits is found around the collapsed caldera. The emplacement of sub-volcanic suites including quartz diorite porphyry, diorite porphyry, and rhyolite porphyry took place at ~144–140 Ma following the eruption of andesitic-dacitic magmas. In the NCC, the volcanism was intense at Late Jurassic contributing to the widespread exposures of volcanic strata referred to as the Tiaojishan Formation (Gao et al., 2012; Duan et al., 2016; Dong et al., 2018; Wu et al., 2019). Another volcanic episode which was dated in the Early Cretaceous (131–127 Ma) is also identified in this area showing a ~15 Ma-temporal gap with earlier eruptions (Figure 6A). They were outcropped at the northern domain of the Sigezhuang pluton (Figure 1C). The Early Cretaceous volcanic rocks (ECVR) are illogical to belong to the Tiaojishan Formation whereas their lithological and geochronological features are consistent with the Zhangjiakou Formation which was majorly distributed in the central and northern margins of the NCC.

In addition to the volcanism, the Early Cretaceous witnessed the magmatic peak in the Laiyuan complex as well (Figure 6A). After the Late Jurassic volcanism and related sub-volcanic emplacement, the Early Cretaceous (~136–126 Ma) intermediate-felsic magmatic event dominated the formation of the Laiyuan complex occurring as concentrically-zoned granitoids that constitute the most of the plutonic-volcanic complex (Figure 1C). Contact boundaries between these synchronous various intrusive suites are legible and clear (Figure 2D) which are called pulsating contact relationship indicating the compositional diversities of granitoids stem from multiple magmatic rather than simple crystallization differentiation of single magma. The MMEs contained in the granitoids were dominated by diorite and quartz monzonite and are simultaneous with the host rocks. It is noteworthy that the MMEs, ECVR, and felsic dykes which all display andesitic-dacitic lithology, were formed at the same time (~131–127 Ma).

Geochronological, petrological, and spatial connections imply their concordance in petrogenesis. They are of different forms (enclaves, dykes, and lavas) but share similar magma sources and petrogenesis.

Mafic dyking events were developed after the major parts of the complex established occurring as dolerite and lamprophyre dykes. Obtained data suggest a long-lived mafic magmatic event in the Laiyuan complex from 125 to 117 Ma generating the dolerite dyke suite (Figure 6A). In contrast to the dolerites, the lamprophyres are characterized by a limited and younger range of ages from 115 to 111 Ma (Figure 6A). Compared with the mafic intrusions, granitoids, and volcanic suites, these tiny dykes only account for insignificant proportions of the complex, however these widespread mafic dyking events throughout the complex and even intruding the country rocks suggest a common and continuous mafic dyking magmatism from 125 to 111 Ma in the NTM (Yang, 1989, 1991; Zhang et al., 2003).

The compiled and new radiometric age data, combined with field observations, define a complicated history of magmatism for the Laiyuan complex, beginning with hornblendite and pyroxenite formation at ~154 Ma, then the first proceeding to eruptions of andesitic-dacitic-rhyolitic lavas at ~146 Ma and emplacement of ore-related sub-volcanic rocks at ~144 Ma, reaching the peak with the intrusion of large, concentrically-zoned granitoids from ~136 to 126 Ma, following the second episode of volcanism at ~130 Ma, and concluding with the tiny but widespread mafic dyking events from ~125 to 110 Ma. To illuminate the spatio-temporal links between diverse magmatic suites is the postulate to investigate the petrogenetic relationships and the in-depth tectonic universality.

5.2 Source variations between diverse magmatic suites

The Lu-Hf isotopic composition of zircon provides significant imprints on the magma source variations. The variations and linkages of Hf isotopic compositions are brought out through the zircon $\varepsilon_{Hf}(t)$ values vs age diagram (Figure 6B). On the whole, the $\varepsilon_{Hf}(t)$ values and Hf crustal model ages for the Laiyuan magmatic rocks are majorly in the ranges of -22.5 to -15.0 and 2.5 to 2.0 Ga, respectively. The negative zircon $\varepsilon_{Hf}(t)$ values generally suggest that the magmas were not solely sourced from juvenile components such as juvenile crust or asthenospheric mantle, and may be primarily sourced from the enriched lithospheric mantle with or without additions from fertile mafic lower crust. This inference is also supported by previous studies of Sr-Nd isotopes and geochemical features (Figures 4G,J) for various magmatic suites from the Laiyuan complex (e.g., Chang et al., 2021). The ultramafic cumulates, mafic intrusions, intermediate-felsic granitoids, and volcanic and sub-volcanic rocks fell near the EMI field in the Sr-Nd isotope diagram (see Chang et al., 2021) suggesting they may share a common basaltic magma derived from an enriched lithospheric mantle probably previously modified due to subduction (Hawkesworth et al., 1993; Foley et al., 2000; Schmidt et al., 2009). The contribution from the enriched lithospheric mantle plays a significant role in the formation of this complex, and this is the source connection throughout different magmatic units.

Despite the similarity in their source, the complexities in the source materials are also recorded in the changes of Hf isotopic compositions (Figure 6B). It is apparent that the zircon $\varepsilon_{Hf}(t)$ values display reverse variation trends at ~130 Ma. From 150 to 130 Ma, the zircon $\varepsilon_{Hf}(t)$ values are decreasing and change from variable to uniform through time, whereas these values are increasing and changing from uniform to variable from 130 to 110 Ma. The distinct variation trends probably result from the involvement of multiple materials including crustal and asthenospheric components. The Late Jurassic volcanic rocks (LJVR) which were formed at ~146 Ma exhibit a variable zircon $\varepsilon_{Hf}(t)$ values ranging from -25 to -10 (Figure 6B). Besides, inherited zircon cores from basement rocks with ages in the range of ~2.65–2.08 Ga are common in these andesitic-dacitic rocks with positive $\varepsilon_{Hf}(t)$ values (0–10) consistent with the values of basement rocks of the Fuping Complex (Figure 6B) suggesting juvenile source synchronous with the major crustal growth in the NCC (Geng et al., 2012; Zhao et al., 2012; Tang et al., 2015; Tang et al., 2016). In terms of the published Sr-Nd-Pb isotopic features, the ~146 Ma volcanic rocks are characterized by low radiogenic Pb and high radiogenic Sr isotopic composition which might result from enriched mantle-derived melts and lower crust melts (Gao et al., 2012). Therefore, the magma source for the LJVR involved both enriched lithospheric mantle and lower crustal components. After ~140 Ma, the intermediate-felsic magmatism which generated the granitoids, the felsic dykes and the ECVR, was intensive and culminated at ~130 Ma. The zircon $\varepsilon_{Hf}(t)$ values for the rocks during this period show a transformation to values ranging from -23.5 to -16.8 especially the ECVR (-23.5– -19.4). Considering the major lithospheric mantle source, this variation trend could be interpreted as the decreasing contribution of crustal materials to the source. As illustrated by the whole rock Sr-Nd isotopes (Chang et al., 2021), the granitoids are plotted in the field closer to the lower crustal components of the NCC than the LJVR suggesting the change of crustal materials. As a result, the decreasing input of lower crustal components accounts for the decreasing trend of zircon $\varepsilon_{Hf}(t)$ values.

The mafic dyke events took place in the complex after ~130 Ma and generated dolerites and lamprophyres showing disparate zircon Hf isotopic compositions. As illustrated in $\varepsilon_{Hf}(t)$ vs age diagram (Figure 6B), the Laiyuan lamprophyres show a wider range of zircon $\varepsilon_{Hf}(t)$ values from -17.2 to -3.7 compared with dolerites (-23.3 to -14.2) suggesting that the sources of lamprophyres are mixed and different from that of the dolerites whose limited negative zircon $\varepsilon_{Hf}(t)$ values suggest that the dolerites were mainly sourced from an ancient enriched

lithospheric mantle. The different incorporation of crustal materials into the lithospheric or asthenospheric mantles can both explain the variable and enriched zircon Hf isotope compositions in the mafic dykes. However, the detailed geochemical studies (Xue et al., 2019b) show that crustal contamination did not play a key role in the ascent of lamprophyres excluding the possibility of much incorporation of crustal materials. The increasing input of asthenospheric material through time is evident in mafic dykes, as indicated by the increasing zircon $\varepsilon_{Hf}(t)$ values from dolerites to lamprophyres compared with mafic dykes from the Jiaodong area (Ma et al., 2014; Ma et al., 2016; Liu S. et al., 2017; Liu et al., 2018). The variation trend is also shown by the signature of whole Sr-Nd isotope compositions (Zhang et al., 2003). The dolerites show more depleted Nd isotopic composition ($\varepsilon_{Nd}(t)$ values ranging from -15.2 to -10.5) and high initial $^{87}Sr/^{86}Sr$ ratios ranging from 0.70523 to 0.70683 than the lamprophyres ($\varepsilon_{Nd}(t)$ ranging from -8.3 to -8.6 and initial $^{87}Sr/^{86}Sr$ ratios ranging from 0.7052 to 0.70554) suggesting that the lithospheric mantle source for mafic dykes and some input of asthenospheric mantle for lamprophyres in Laiyuan area as well (Chang et al., 2021). As a consequence, in terms of isotopic evidence, the increasing trend of zircon $\varepsilon_{Hf}(t)$ values from dolerites to lamprophyres demonstrates the increasing involvement of asthenospheric mantle into the lithospheric mantle through time contributed to the source of mafic dykes.

In summary, the enriched lithospheric mantle accounts for the major magma source for the ultramafic-mafic rocks, intermediate-felsic granitoids, volcanic rocks and mafic dyke suites from ~150 to 110 Ma. Over a long time, multiple sources e.g. asthenospheric materials and crustal melts, are involved in this formation process. From 150 to 130 Ma, the lower crustal contribution to the source shows a decrease from the LJVR, through granitoids, to the ECVR and felsic dykes whereas the asthenospheric mantle contribution is increasing through time from dolerites to lamprophyres during 130–110 Ma.

5.3 Crust-mantle interaction

According to the temporal and source variations of diverse magmatic suites, the petrogenesis from different rocks could be summarized. As for granitoids, they could be classified into two groups based on their geochemical features (Xue et al., 2021) including the granitic and monzonitic rocks. The high-K calc-alkaline I-type monzogranites were generated by partial melting of the mafic lower crust while the monzonitic rocks have experienced a two-stage magmatic evolution of the first plagioclase-dominated fractional crystallization from lithospheric mantle-derived mafic magma and the second amphibole-dominated fractional crystallization to form the evolved monzonitic magma with adakitic geochemical features (Chang et al., 2021; Xue et al., 2021). Similarly, the eruptive rocks shared a similar genetic process with the monzonitic rocks thus they could also exhibit adakitic affinities (Gao et al., 2012; Xue et al., 2020). In terms of MMEs, unique petrological textures (Chen et al., 2009), the large variations of elements and $Mg^{\#}$ values (40–60, Xue et al., 2021), and isotopic imprints (Hf isotopes) (Chen et al., 2009) support the mixing origin of lower crust-derived felsic magma and lithospheric mantle-sourced dioritic magma for the MMEs from the Laiyuan complex. Furthermore, the underplated mantle-derived mafic magma could also experience magmatic evolution to form the gabbro and cumulative ultramafic rocks (Chang et al., 2021). In conclusion, intense mantle and crustal magmatic processes have been identified in the formation of the Laiyuan magmatic complex. Above detailed petrological, geochemical, isotopic, and geochronological research have illustrated that the incorporation of the thickened lower crust and enriched lithospheric mantle in the source, and the involvement of diverse magmatic processes, have played a significant role in the petrogenesis of the Laiyuan igneous complex arousing the heterogeneities.

Above detailed petrological, geochemical, isotopic, and geochronological research have illustrated that the incorporation of the thickened lower crust and enriched lithospheric mantle in the source, and the involvement of diverse magmatic processes including the partial melting of variable sources, fractional crystallization, magma mixing and mingling, and crystal accumulation and compaction, have played a significant role in the petrogenesis of the Laiyuan igneous complex. It could be attributed to the crust-mantle interaction contributing to the formation of the Laiyuan magmatic complex (Figure 7A). The mantle-derived underplated mafic magmas act as not only the thermal source to induce the crustal melting, but also the mafic end-member to interact with the felsic melts/magmas derived from the crust. As a result, a series of magmatic rocks with compositional heterogeneity were formed, including mafic-ultramafic rocks and felsic rocks in the forms of eruption, plutonic emplacement, enclave, and felsic dyke (Figure 7A). In the central NCC, such magmatic complexes (plutons) similar to the Laiyuan complex, such as the Dahenan complex (Chen et al., 2009) and Mapeng pluton (He and Santosh, 2014) from the NTM, and the Fushan pluton (Li et al., 2019) from the STM, are widespread indicating that the intense crust-mantle interaction is the common deep process beneath the intra-domain of the NCC. The crust-mantle interaction took place during Late Mesozoic, peaking at the Early Cretaceous, consistent with the NCC destruction peaking period (Zhang et al., 2014; Liu et al., 2019; Wu et al., 2019) revealing the tight internal genetic relationship between the magmatism, interaction, and destruction. In brief, the deep crust-mantle interaction holds important clues to the Mesozoic tectonic setting and craton destruction mechanism in the central NCC. Complex source materials and multiple magmatic evolutional processes

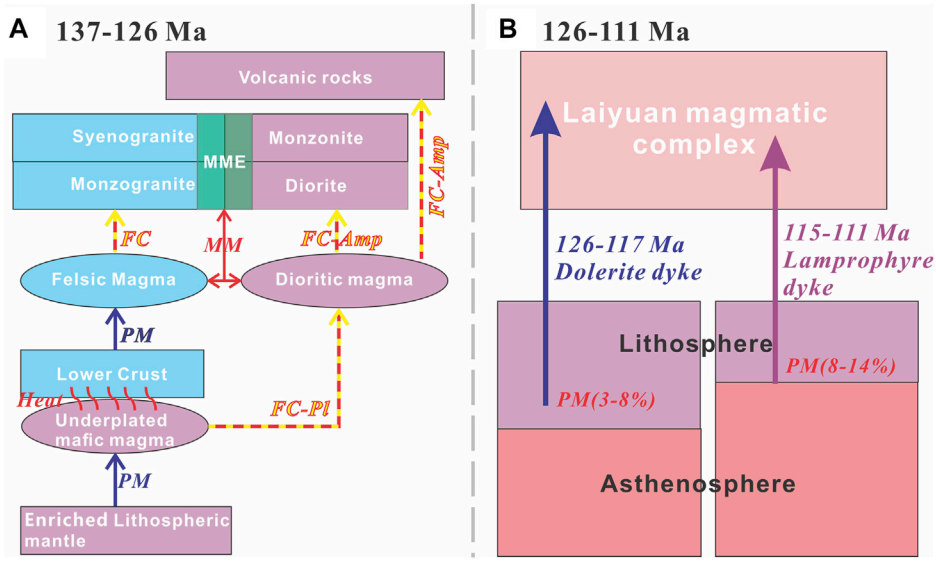

FIGURE 7
Schematic cartoon (not to scale) illustrating the crust-mantle interaction accounting for the formation of Laiyuan granitoid intrusion and Early Cretaceous volcanic rocks from 137 to 126 Ma **(A)**, and lithosphere-asthenosphere interaction accounting for the generation of dolerite and lamprophyre dyke during 126–111 Ma **(B)**. See context for detailed interpretation. Abbreviations: FC-Amp: amphibole-dominated fractional crystallization; FC-Pl: plagioclase-dominated fractional crystallization; MM: magma mixing; PM: partial melting and the values represent the degrees of partial melting.

contributed to the compositional diversity of the Laiyuan complex (Figure 7A).

5.4 Lithosphere-asthenosphere interaction

The above source discussion has demonstrated the input of the asthenospheric mantle is increasing from dolerite dykes (126–117 Ma) to lamprophyre dykes (115–111 Ma) indicating the magma sources for mafic dykes have changed from the enriched lithospheric mantle to the enriched lithospheric mantle+asthenospheric mantle (Xue et al., 2019b). In addition, the Dy/Yb ratios are useful to evaluate the source nature and degree of partial melting of mafic dykes (Ma et al., 2016). From dolerite to lamprophyre, the Dy/Yb ratios are decreasing from 2.66–3.21 to 2.45 to 2.65 (Xue et al., 2019b) suggesting the melting depths have shifted from 80 to 100 km (Garnet stability field) to ~80 km (Garnet-spinel transitional field), and the degrees of partial melting of the lithospheric mantle are increasing from 3%–8% to 8%–14% (Duggen et al., 2005; Mckenzie and O'Nions, 1991; Robinson and Wood, 1998; Yang et al., 2010). All these variations could be interpreted by the lithosphere thinning and the asthenosphere upwelling with the fact that the asthenosphere cannot melt until the thickness of the lithosphere has been reduced to less than about 80 km. Furthermore, by comparing with isotopic (e.g., $\varepsilon_{Hf}(t)$ values, Figure 6B) and geochemical features (e.g., TiO_2 contents and Nb/La ratios, not shown) of asthenospheric mantle-derived and lithospheric mantle-derived mafic dykes from Jiaodong areas (Ma et al., 2014; Ma et al., 2016; Xue et al., 2019b), the Laiyuan mafic dykes show special "transitional" features indicating the lithosphere-asthenosphere interaction could be interpreted as the possible petrogenesis for mafic dykes in the central NCC (Figure 7B). In this case, the lithosphere-asthenosphere interaction means the partial melting of the asthenospheric mantle interacted with the eroded lithospheric mantle material to produce the lamprophyre dykes in the Laiyuan complex similar to the Datong Cenozoic basalts from Datong Volcanic Field near Laiyuan area (Xu et al., 2005). In addition, the lithosphere-asthenosphere interaction exhibits smooth and gradual characteristics which are distinct from the intense and rapid mafic diking events in Jiaodong area during the Mesozoic indicating the different lithospheric evolutions (Ma et al., 2014).

6 Tectonic implications

6.1 Tectonic regime transition from compression to extension

In the eastern and central NCC, three metallogenic pulses are identified, i.e. 200-160 Ma, ca. 140 Ma, and 130–110 Ma when the tectonic regime was under post-collisional setting,

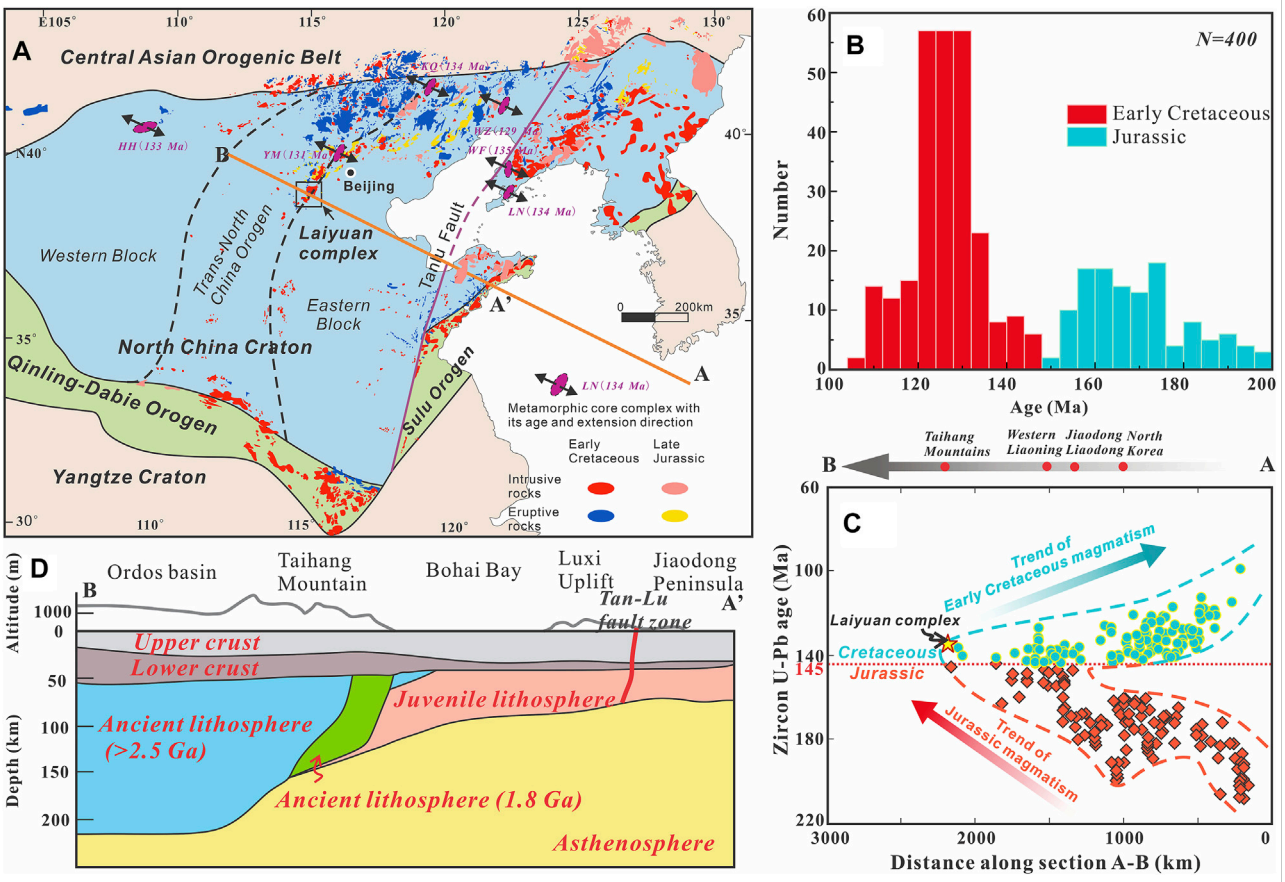

FIGURE 8
(A) Tectonic map of the North China Craton and surrounding regions showing the metamorphic core complex (modified after Zhu et al., 2015) and Early Cretaceous and Late Jurassic magmatic rocks (Zhao et al., 2005; Zhang et al., 2014). **(B)** Histogram of zircon U-Pb ages of Late Mesozoic igneous rocks in the NCC. **(C)** Projection of zircon U-Pb ages along section A-B (in Figure 8A) cross the NCC. The combinations of the zircon U-Pb ages are modified after Wu et al. (2019) and reference therein. **(D)** The schematic lithospheric structure of the current NCC from the eastern Jiaodong Peninsula through the central Taihang Mountain (A′-B in Figure 8A, not to scale) to the western Ordos Basin revealing the lithosphere heterogeneity beneath the NCC (modified after Liu et al., 2019). Metamorphic core complex: KQ-Kalaqing metamorphic core complex; WZ-Waziyu metamorphic core complex; LN-Liaonan metamorphic core complex; WF- Wanfu metamorphic core complex; YM-Yunmengshan metamorphic core complex; FS-Fangshan metamorphic core complex; HH-Hohhot metamorphic core complex.

transforming from compression to extension, and intense extensional setting, respectively (Mao et al., 2005). The significant tectonic regime transformation from Late Jurassic to Early Cretaceous was also recorded by the widespread metamorphic core complex in the NCC (Wang et al., 2012) (Figure 8A). Detailed geochronological studies of the Yunmengshan metamorphic core complex illustrate a rapid change in the tectonic setting from NNE-SSW compression to NW-SE extension in the earliest Cretaceous (Zhu et al., 2015). In the study area, geochronological studies on the Mujicun deposit show that the volcanic rocks, porphyry intrusion, and porphyry-type and skarn-type of mineralization were formed during the same event at 145–140 Ma consistent with the important tectonic regime changing period (Gao et al., 2012; Gao et al., 2013; Dong et al., 2013; Hou et al., 2015) similar to the skarn-porphyry Cu-Mo and Mo-W mineralizations in Jiaodong area (Goldfarb and Santosh, 2014) and East Qinling orogen (Li et al., 2018; Yang et al., 2019b). Furthermore, the LJVR belongs to the Tiaojishan Formation which was also regarded as the intra-plate volcanism induced by the transition in the tectonic regime (Dong et al., 2018). Therefore, the early formation of the Laiyuan complex was associated with the tectonic regime transition from compression to extension accompanied by the formation of LJVR, sub-volcanic rocks, and hosted Cu-Mo mineralization.

Lithospheric extension beneath eastern China during the Early Cretaceous is supported by several lines of evidence, including a series of fault basins, numerous detachment faults, metamorphic core complexes, and associated voluminous magmatism (Zhu et al., 2011) (Figure 8A). Compared with the Jurassic magmatism, the Early Cretaceous magmatism was

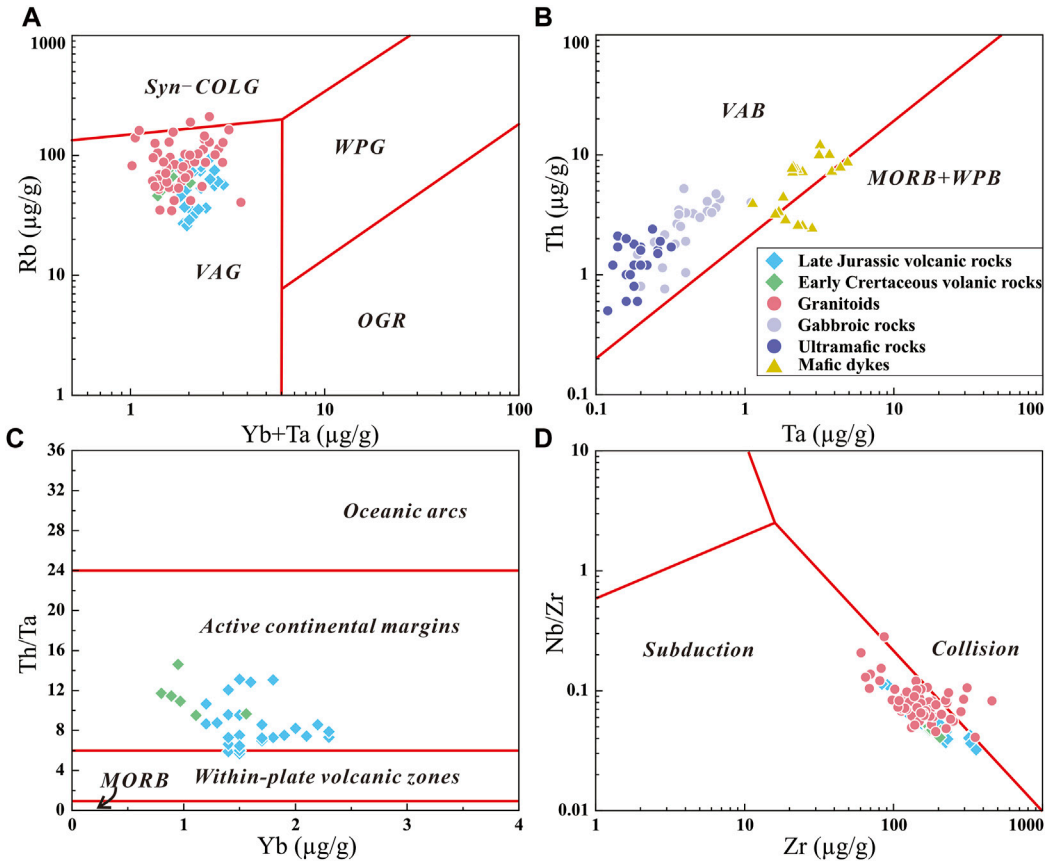

FIGURE 9
Tectonic discriminative diagrams for magmatic rocks from the Laiyuan complex. **(A)** Rb vs Yb+Ta diagram (Pearce, 1984). **(B)** Th vs Ta diagram (Pearce and Peate, 1995). **(C)** Th/Ta vs Yb diagram (Pearce and Peate, 1995). **(D)** Nb/Zr vs Zr diagram (Tarney and Jones, 1994). Data source are same as in Figure 4.

more intense and widespread throughout the eastern and central NCC marking the peak of the extension (Figures 8A, B). Apparently, the Early Cretaceous intense magmatism in the study area displays a close relationship with the extensional setting because the lithosphere-asthenosphere and crust-mantle interaction to generate the Laiyuan magmatic complex are commonly marking deep extension architecture (Campos et al., 2012; Orozco-Garza et al., 2013; Li et al., 2014; Deng et al., 2017). To interpret the trigger of the extensional tectonic regime, several mechanisms have been presented. Among the two popular models, one relates the Triassic collision between the NCC and Yangtze Block with the intra-continental extensional regime during the post-collision (Zhang et al., 2002). The other model proposes the nearly W-E subduction of the Paleo-Pacific Ocean which changed the geodynamic regime from N-S transpressional setting to nearly W-E extensional setting (Li and Santosh, 2017). A marked age polarity has been identified in the East Asian magmatic suites with a northwestward younging trend from Japanese islands (~210 Ma), through the Jiaodong and Liaodong areas (180 Ma), to the Taihang Mountain in central NCC (138 Ma), which has been linked with the subduction process of Paleo-Pacific Plate (Chen et al., 2005), with extension of the NCC triggered by the subduction process.

6.2 Geodynamic trigger for the NCC destruction

Before discussing the possible mechanism for the NCC destruction, the prior focus is the tectonic triggering forces for the destruction. Previous studies show that the subduction of the oceanic plate and plume erosion act as the major driving force for craton destruction in the margins or within continental interiors, respectively (Wilde et al., 2003; Menzies et al., 2007). As shown in the tectonic setting discriminative diagrams (Figure 9), the rocks from the Laiyuan complex are showing subduction-related characteristics. As well, the rocks exhibit geochemical features similar to the rocks generated in active continental margins

(Figure 9). However, these rocks were formed far from any active continental margin arc setting during the Mesozoic and show an intra-plate setting as also suggested in previous studies from the TM and north Hebei Province (Gao et al., 2011; He et al., 2017; Dong et al., 2018; Li et al., 2019; Yang et al., 2020). The arc-like characteristics might be an inheritance from the lithosphere beneath the central NCC which was influenced by the oceanic plate subduction through far-field effects (He et al., 2017). As well, the granitoids plotted in the VAG field (Figure 9A), and the mafic rocks fell in the field of active continental margin (Figures 9B, C) indicating the primary controlling effect exerted by subduction to form the magmatic rocks in the central NCC. The following lines of evidence support that the NCC destruction was triggered by the subduction of the Paleo-Pacific Plate, neither by the subduction of the Paleo-Asian oceanic plate to the north nor the subduction of the Paleo-Tethys and following the continental collision between the NCC and Yangtze Craton to the south (Windley et al., 2010). Firstly, the NCC experienced extensive destruction in its eastern and central parts showing a gradual thinning trend from west to east whereas the western part still has a thick and stable lithosphere suggesting the subduction effect came from the east (Chen, 2010). Secondly, combined age data of Mesozoic magmatic rocks from the NCC (Figure 8C) show that the Jurassic calc-alkali magmatism exhibits a westward younging trend, whereas the Cretaceous calc-alkali magmatism shows a reverse eastward younging trend, indicating the role of subduction and rollback of the Paleo-Pacific Plate in the spatial-temporal migration of Mesozoic magmatism in the NCC (Wu et al., 2019). Thirdly, there are northeast-extending belts of the Mesozoic magmatic rocks and contemporaneous sedimentary basins distributed parallel to the subduction zone of the Paleo-Pacific Plate (Li et al., 2012; Wang et al., 2012) (Figure 8A). Therefore, the subduction of the Paleo-Pacific Plate exerted a principle influence on the thinning, extension, and destruction of the NCC.

Based on previous studies and this study, some key stages associated with the subduction of the Paleo-Pacific Plate can be recognized: initiation of the subduction beneath Northeast China between ~200–190, low-angle flat subduction between ~170 and 145 Ma, the sinking or rollback between ~145–110, stagnancy and vanish of Paleo-Pacific slab in the mantle transition zone at ~110–50 Ma (Liu et al., 2019; Wu et al., 2019; Zhu and Xu, 2019). During Late Jurassic, at ca. 155 Ma, the Paleo-Pacific Plate began to roll back, with the tectonic setting changing from compression to extension. By ~145 Ma, the slab had mostly rolled back contributing to unstable mantle flows and upwelling of the asthenosphere. In summary, the westward subduction, retreat, rollback and stagnation of the Paleo-Pacific Plate are the deep driving force of the NCC destruction resulting in the heterogeneous lithosphere and various evolutional processes in the deep beneath the NCC, furthermore manifested as distinct magmatic rocks series in the shallow.

6.3 Different lithospheric evolution beneath the eastern and central NCC

Seismic data indicate that the present lithospheric thickness of the NCC becomes gradually reduced from the Western Block (~200 km in the Ordos basin) through the central region (120 km in the TM) to the Eastern Block (only 70 km in the Bohai Bay region) (Chen, 2010). The geophysical data also reveals the crustal structure is varying from the eastern to the central NCC, with the thickness of the lower crust decreasing from ~20 km in the TM to only 6 km in the Bohai Bay (Zheng et al., 2007). In addition, by studying the Cenozoic basalts and hosted xenoliths, the ancient lithosphere in the eastern NCC has been replaced by juvenile lithosphere while just a small portion of the lithosphere ancient has changed to juvenile materials and the ancient lithosphere still dominated (Liu et al., 2019; Wu et al., 2019) (Figure 8D). These differences in thickness and structure essentially reflect the spatial variation of lithospheric evolution throughout the NCC.

The magmatic similarities in both central and eastern NCC reveal the consistency of lithospheric evolution by the Late Jurassic. However, distinct from Jurassic magmatism, the Early Cretaceous magmatism occurred more widely, resulted in extremely variable rock types and chemical compositions, and involved multiple crustal and mantle sources (Zheng et al., 2018; Wu et al., 2019). The crust-mantle interaction played a significant role during their formation in both central and eastern NCC, but may be of different forms. As discussed in this study, the underplated basaltic magma derived from the enriched lithospheric mantle interacted with the thickened lower crust to account for the variable magmatic rocks in the central NCC (bottom to up), whereas the melts derived from the delaminated lower crust interacted with the overlying mantle peridotite contributed to the formations of high-Mg andesites and adakites in the eastern NCC (up to bottom) (Gao et al., 2004; Jiang et al., 2007; Gao et al., 2009; Xu et al., 2013). The different forms of crust-mantle interaction are consistent with the thickness variations of the lithosphere.

Notably, the mafic dyke events that occurred in both regions offered direct evidence to identify the distinct lithospheric evolution. Two types of lamprophyres with the same emplacement ages of ca. 121 Ma have been discovered in the Jiaojia gold deposit from the Jiaodong region (Ma et al., 2014; Deng et al., 2017): one is the high-Ti lamprophyres sourced from the partial melting of an asthenospheric mantle with juvenile and depleted isotopic characteristics ($\varepsilon_{Hf}(t)$ values ranging from -4.7 to 2.1), another is the low-Ti lamprophyres sourced from the lithospheric mantle with ancient and enriched isotopic features ($\varepsilon_{Hf}(t)$ values ranging from -29.3 to -23.1) (Figure 6B). The co-occurrence of the two types of lamprophyres records a rapid transition from lithospheric to asthenospheric mantle sources, indicating the rapid detachment of the lithosphere and rapid upwelling of the asthenosphere

beneath the eastern NCC (Ma et al., 2016; Deng et al., 2017). However, as revealed by the increasing input of asthenospheric materials through time for the source of lamprophyres from 115 to 111 Ma, and the relatively uniform enriched lithospheric mantle source for the dolerites from 125 to 117 Ma, a progressive and slow lithospheric thinning and asthenospheric upwelling process occurred at the central NCC. The distinct lithospheric evolutional processes in the central and eastern NCC may result from the different destruction mechanisms and lead to the different lithospheric evolution beneath the central and eastern NCC at present.

6.4 Destruction mechanism in the central NCC

Several models were proposed to interpret the destruction process including convective destabilization (Houseman et al., 1981; Morency et al., 2002), tectonic erosion (Maruyama et al., 2007; Santosh, 2010), destabilization due to the Indo-Eurasian collision (Menzies et al., 2007), thermo-mechanical erosion (Griffin et al., 1998; Xu, 2001), and continental delamination (Gao et al., 2004; Windley et al., 2010). Among these models, thermo-mechanical erosion and lithospheric delamination modes are the more accepted mechanisms to explain the lithospheric thinning process. These two models have contrasting characteristics of magmatic imprints. In the case of thermo-mechanical erosion, the upwelling asthenosphere gradually heats up, weakens, and erodes the lowermost lithosphere (Xu et al., 2005; Xu et al., 2009). Progressive removal would contribute to considerable thinning of the lithosphere (Ma et al., 2016). The magmatism related to this process will have lithospheric mantle features at the beginning, followed by asthenospheric mantle characteristics with progressive thinning (Xu et al., 2009; Cai et al., 2013). The formation of the Laiyuan magmatic complex perfectly fits such characteristics. At early stage, the lithospheric mantle-derived magmas underplated the crust to generate the mafic rocks, andesitic volcanic rocks, and granitoids. Gradually, the clues of the asthenospheric mantle are increasing in the dolerites and lamprophyres. The smooth and progressive transition process indicates the case of thermo-mechanical erosion in the central NCC. In contrast, the delamination model hypothesizes that thickened lower crust and the coupled lithosphere sunk into the convective asthenospheric mantle to produce simultaneous lithospheric and asthenospheric mantle-derived magmas as well as mixed felsic magmas (Gao et al., 2004; Wu et al., 2008). The two types of mafic dykes in the Jiaodong area (Ma et al., 2014; Deng et al., 2017), and the formation of high-Mg adakitic rocks and mafic dykes from different sources in the proximal western Shandong region (Liu S. et al., 2017; Li et al., 2017) indicate the delamination of lithosphere can be well demonstrated in the eastern NCC. Furthermore, given the different lithospheric nature (Figure 8D), it is difficult to use the delamination model to interpret the formation of Mesozoic magmatic rocks in the central NCC whereas it is reasonable to apply the thermal-mechanical erosion to account for the craton destruction in the central NCC. The lithosphere-asthenosphere and crust-mantle interactions constitute the vertical craton destruction phenomenon induced by thermal-mechanical erosion. The delaminated lower crust cannot pass through the thick lithospheric mantle to founder into the asthenosphere because of the buoyancy and strength in the central NCC.

In summary, it could be concluded that the thermal-mechanical erosion happened in the Central NCC, and lithospheric delamination took place in the eastern NCC. The lithosphere experienced different evolutional processes in the NCC. In the central NCC, gradual erosion and replacement of ancient lithosphere happened to lead to most of the ancient lithosphere has been preserved. However, in the eastern NCC, the ancient lithosphere was rapidly delaminated and was totally replaced by the juvenile lithosphere. Both two mechanisms played a significant role in the NCC destruction process to form variable magmatic rocks. Although the two mechanisms certainly differ from each other, the connection between them cannot be eliminated. The rapid and intense lithospheric delamination would trigger thermo-mechanical erosion within the interior domains of the NCC, and the slow and gradual erosion would act as the preclusion of large-scale delamination.

6.5 An integrated petrogenetic model for the Laiyuan complex

Combining the spatial, temporal, genetic, and tectonic linkages, considering the state change of the Paleo-Pacific slab beneath the NCC, an integrated petrogenetic model has been proposed to describe the magmatic evolution of the Laiyuan magmatic complex (Figure 10). Both the two mechanisms combined with the Paleo-Pacific slab played a significant role in the NCC destruction process to form variable magmatic rocks.

During Early Jurassic (~200 Ma), the initiation of subduction of the Paleo-Pacific Plate occurred beneath Northeast Asia (Ma and Xu, 2021). Until ~150 Ma, the slab has reached the position beneath the central NCC. The cold slab lowered the geothermal gradient of the mantle beneath the craton and depressed direct mantle melting. During this period, the central NCC was under compression which thickened the lithosphere in the central NCC. The LJVR with the sub-volcanic suites corresponding to Tiaojishan Formation were formed during this period whose petrogenesis could be attributed to the MASH process (melting, assimilation, storage, homogenization) highlighting the important role of partial melting of the thickened lower crust (Hildreth and Moorbath, 1988; Gao et al., 2012). The deep hornblende-dominated fractional crystallization process accounts for the sporadic ultramafic cumulates and evolved

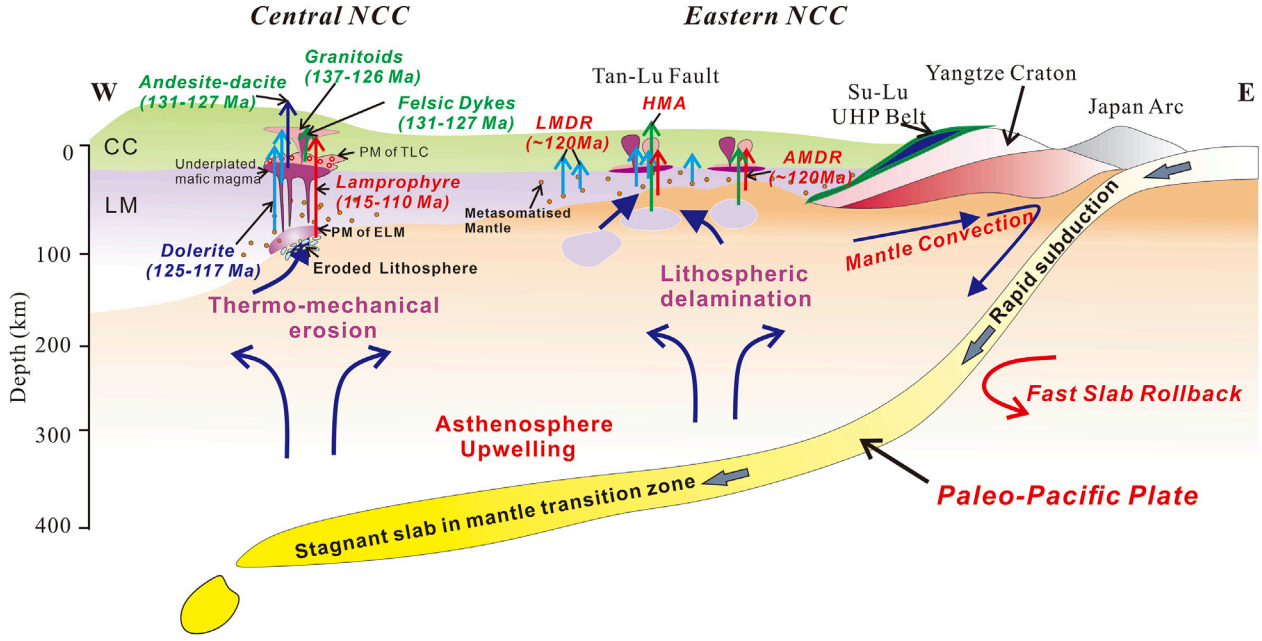

FIGURE 10
Schematic plate tectonic model (not to scale) to explain the lithospheric destruction of the North China Craton during Early Cretaceous through thermal-mechanical erosion and lithospheric delamination. Detailed discussions are in the text. AMDR, asthenospheric mantle-derived rocks; CC, continental crust; ELM, enriched lithospheric mantle; HMA, high-Mg adakites; LM, lithospheric mantle; LMDR, lithospheric mantle-derived rocks; TLC, thickened lower crust.

andesitic magmas with adakitic affinities which ascend through the crust to erupt.

During 145–140 Ma, fast slab rollback occurred leading to hot asthenosphere upwelling and extensional setting in the central NCC. This intense mantle convection transformed from central to eastern NCC identified by the eastward younging trend of magmatism after ~140 Ma (Figure 8C). Induced by the upwelling of hot asthenosphere, the pre-weakened metasomatized lithospheric mantle would be heated and eroded, which would lead to partial melting, producing the parental basaltic magma. These magmas would be underplated beneath the base of the thickened lower crust, acting as not only the thermal source to induce the crustal melting, but also the mafic end-member to interact with the felsic melts/magmas derived from the crust. The intense and consistent crust-mantle interaction accounts for the petrogenesis for the formation of the Laiyuan magmatic complex, including granitoids (136–126 Ma), MMEs (129–126 Ma), ECVR (131–127 Ma), and felsic dykes (131–127 Ma). The compositional heterogeneities of the igneous complex resulted from the multiple involved mantle and crustal sources, chaotic mixing and mingling process, and the complicated fractional crystallization during the deep interaction process.

From 145 to 110 Ma, the lithosphere in the central NCC underwent continued thinning and erosion. Through time, the lithosphere became substantially thin, and lithospheric mantle-derived magmas could migrate through the lithospheric faults and intrude the plutons or country rocks leading to the formation of dolerite dykes at 125–117 Ma. The continuous asthenospheric upwelling caused heterogeneous erosion along weak zones resulting in non-uniform destruction of the lithosphere. In the eastern NCC, at ~120 Ma, delamination of the eclogitic lower crust occurred and the evacuated mantle was replaced by hot asthenosphere. However, in the central NCC, the delamination didn't happen but the thermal-mechanical erosion took place to generate eroded lithosphere. Following delamination in the Jiaodong area at ~120 Ma, and the rapid slab rollback induced intense mantle convection, with further input from the accumulating slab graveyards in the mantle transition zone, the mantle upwelling and thermo-mechanical erosion reached their peak. The continuous lithospheric thinning eventually resulted in the upwelling asthenosphere reaching the depth where it could melt (80 km). More asthenosphere mantle began to melt with eroded lithospheric mantle. The partial melting of the asthenospheric mantle and its interaction with the lithospheric mantle material produced the lamprophyre with

both arc-type and OIB-type characteristics dykes from ~115 Ma to 111 Ma.

Thus, the above discussion interprets the integrated formation process of the Laiyuan magmatic complex. This formation mechanism could be also used to account for the petrogenesis of the magmatic plutons in the central. It is favored that both of the lithospheric delamination and thermo-mechanical erosion together played a key role in the destruction of the cratonic architecture of the NCC (Figure 10).

7 Conclusion

The complex evolutionary history of magmatism in the Laiyuan complex began with ultramafic cumulate formation, followed by eruption of andesitic-dacitic lavas at ~146 Ma, and a peak of intrusion of granitoid and simultaneous small mafic rocks from ~136 to 126 Ma, following the second episode of volcanism at ~130 Ma, and finally minor but widespread mafic dyking events from ~125 to 110 Ma. The isotopic data show that the enriched lithospheric mantle accounts for the major parental magma source for the Laiyuan magmatic rocks ~150–111 Ma. Over a long time, multiple sources e.g., asthenospheric materials and crustal melts, are involved in this formation process.

Intense crust-mantle interaction incorporating the thickened lower crust and enriched lithospheric mantle in the source, and the involvement of diverse magmatic processes including the partial melting of variable sources, fractional crystallization, and magma mixing and mingling played a significant role in the petrogenesis of the Laiyuan igneous complex. Thus, a series of magmatic rocks with compositional heterogeneity were formed, including mafic-ultramafic rocks and felsic rocks in the forms of eruption, plutonic emplacement, enclave, and felsic dyke. Furthermore, the gradual and smooth lithosphere-asthenosphere interaction accounts for the formation mechanism of mafic dykes in the central NCC.

The intense magmatism to form the Laiyuan complex was under the extensional tectonic setting triggered by the subduction of the Paleo-Pacific Plate. The different lithospheric evolution beneath the eastern and central NCC during the Early Cretaceous resulted from different destruction mechanisms. A slow and gradual thermal-mechanical erosion occurred at the central NCC, whereas rapid and intense lithospheric delamination occurred at the eastern NCC. Both of the mechanisms combined with the Paleo-Pacific slab subduction played a significant role in the NCC destruction process generating different magmatic suites.

Author contributions

FX: Conceptualization, Data curation, Formal analysis, Methodology, Writing-original draft, Writing-Review and Editing. MS: Data curation, Investigation, Funding acquisition, Supervision, Writing-Review and Editing. TT: Supervision, Writing-Review and Editing. FY: Funding acquisition, Investigation, Writing-Review and Editing. HT: Funding acquisition, Writing-Review and Editing. GC: Writing-Review and Editing; CL: Writing-Review and Editing. YX: Investigation.

Funding

This project was jointly supported by the Second Tibetan Plateau Scientific Expedition and Research Program (STEP) (2022QZKK0202), the Fundamental Research Funds for the Central Universities (Grant No. B210201004), the Fundamental Research Funds for the Central Universities (Grant No. B220202054), and the Opening Foundation of Key Laboratory of Mineral Resources in Western China (Gansu Province) (Grant No. MRWCGS-2021–01).

Acknowledgments

We thank the Editor. ZL and three reviewers for their constructive comments, which helped improve our paper. SW. Kim is thanked for his help in the experiments and discussion.

Conflict of interest

The authors declare that the research was conducted in the absence of any commercial or financial relationships that could be construed as a potential conflict of interest.

Publisher's note

References

Annen, C., Blundy, J. D., and Sparks, R. (2006). The Genesis of intermediate and silicic magmas in deep crustal hot zones. *J. Petrology* 47 (3), 505–539. doi:10.1093/petrology/egi084

Bateman, P. C., and Chappell, B. W. (1979). Crystallization, fractionation, and solidification of the Tuolumne intrusive series, yosemite national park, California. *Geol. Soc. Am. Bull.* 90 (5), 465–482. doi:10.1130/0016-7606(1979)90<465:cfasot>2.0.co;2

Cai, J. H., Yan, G. H., Chang, Z. S., Wang, X. F., Shao, H. X., Chu, Z. Y., et al. (2003). Petrological and geochemical characteristics of the Wanganzhen complex and discussion on its Genesis. *Acta Petrol. Sin.* 19 (1), 81–92. doi:10.3969/j.issn.1000-0569.2003.01.009

Cai, Y. C., Fan, H. R., Santosh, M., Hu, F. F., Yang, K. F., and Li, X. H. (2018). Decratonic gold mineralization: Evidence from the Shangzhuang gold deposit, eastern North China Craton. *Gondwana Res.* 54, 1–22. doi:10.1016/j.gr.2017.09.009

Cai, Y., Fan, H. R., Santosh, M., Liu, X., Hu, F. F., Yang, K. F., et al. (2013). Evolution of the lithospheric mantle beneath the southeastern North China Craton: Constraints from mafic dikes in the Jiaobei terrain. *Gondwana Res.* 24 (2), 601–621. doi:10.1016/j.gr.2012.11.013

Campos, R. S. D., Philipp, R. P., Massonne, H., and Chemale, F. (2012). Early post-collisional Brasiliano magmatism in Botuverá region, Santa Catarina, southern Brazil: Evidence from petrology, geochemistry, isotope geology and geochronology of the diabase and lamprophyre dikes. *J. S. Am. Earth Sci.* 37, 266–278. doi:10.1016/j.jsames.2012.02.005

Chang, J., Audétat, A., and Li, J. (2021). *In situ* reaction-replacement origin of hornblendites in the early cretaceous laiyuan complex, north China craton, and implications for its tectono-magmatic evolution. *J. Petrology* 62 (5), egab030. doi:10.1093/petrology/egab030

Chen, B., Chen, Z. C., and Jahn, B. M. (2009). Origin of mafic enclaves from the Taihang Mesozoic orogen, north China craton. *Lithos* 110 (1-4), 343–358. doi:10.1016/j.lithos.2009.01.015

Chen, B., Jahn, B. M., Arakawa, Y., and Zhai, M. G. (2004). Petrogenesis of the mesozoic intrusive complexes from the southern Taihang orogen, north China craton: Elemental and Sr–Nd–Pb isotopic constraints. *Contrib. Mineral. Pet.* 148 (4), 489–501. doi:10.1007/s00410-004-0620-0

Chen, B., Jahn, B. M., and Suzuki, K. (2013). Petrological and Nd-Sr-Os isotopic constraints on the origin of high-Mg adakitic rocks from the North China Craton: Tectonic implications. *Geology* 41 (1), 91–94. doi:10.1130/g33472.1

Chen, B., Tian, W., Jahn, B. M., and Chen, Z. C. (2008). Zircon SHRIMP U–Pb ages and *in-situ* Hf isotopic analysis for the Mesozoic intrusions in South Taihang, North China craton: Evidence for hybridization between mantle-derived magmas and crustal components. *Lithos* 102 (1), 118–137. doi:10.1016/j.lithos.2007.06.012

Chen, B., Tian, W., Zhai, M. G., and Arakawa, Y. (2005). Zircon U-Pb geochronology and geochemistry of Mesozoic magmatism in the Taihang Mountains and other places of the North China Craton, with implications for petrogenesis and geodynamic setting. *Acta Petrol. Sin.* 21 (1), 13–24. doi:10.3321/j.issn:1000-0569.2005.01.002

Chen, B., and Zhai, M. (2003). Geochemistry of late Mesozoic lamprophyre dykes from the Taihang Mountains, north China, and implications for the sub-continental lithospheric mantle. *Geol. Mag.* 140 (1), 87–93. doi:10.1017/s0016756802007124

Chen, B., Zhai, M., and Shao, J. A. (2003). Petrogenesis and significance of the mesozoic north Taihang complex: Major and trace element evidence. *Sci. China Ser. D.* 46 (9), 941–953. doi:10.1360/02yd0447

Chen, L. (2010). Concordant structural variations from the surface to the base of the upper mantle in the North China Craton and its tectonic implications. *Lithos* 120 (1), 96–115. doi:10.1016/j.lithos.2009.12.007

Chen, Z. C., Chen, B., and Tian, W. (2007). Hf isotopic compositions and geological significance; a case study of Mesozoic batholiths and mafic enclaves in North Taihang. *Acta Petrol. Sin.* 23 (2), 295–306. doi:10.3969/j.issn.1000-0569.2007.02.010

Coleman, D. S., Gray, W., and Glazner, A. F. (2004). Rethinking the emplacement and evolution of zoned plutons: Geochronologic evidence for incremental assembly of the Tuolumne Intrusive Suite, California. *Geol.* 32 (5), 433–436. doi:10.1130/g20220.1

Defant, M. J., and Drummond, M. S. (1990). Derivation of some modern arc magmas by melting of young subducted lithosphere. *Nature* 347 (6294), 662–665. doi:10.1038/347662a0

Deng, J., Liu, X. F., Wang, Q. F., Dilek, Y., and Liang, Y. Y. (2017). Isotopic characterization and petrogenetic modeling of early cretaceous mafic diking—lithospheric extension in the North China craton, eastern Asia. *GSA Bull.* 129 (11-12), 1379–1407. doi:10.1130/b31609.1

Dong, G. C., Santosh, M., Li, S., Shen, J., Mo, X., Scott, S., et al. (2013). Mesozoic magmatism and metallogenesis associated with the destruction of the North China Craton: Evidence from U–Pb geochronology and stable isotope geochemistry of the Mujicun porphyry Cu–Mo deposit. *Ore Geol. Rev.* 53 (3), 434–445. doi:10.1016/j.oregeorev.2013.02.006

Dong, S. W., Zhang, Y., Li, H., Shi, W., Xue, H., Li, J., et al. (2018). The yanshan orogeny and late mesozoic multi-plate convergence in east asia—commemorating 90th years of the "yanshan orogeny". *Sci. China Earth Sci.* 61 (12), 1888–1909. doi:10.1007/s11430-017-9297-y

Duan, C., Mao, J. W., Xie, G. Q., Chen, Z. K., Ma, G. X., Wang, Z. M., et al. (2016). Zircon U-Pb geochronologicl and Hf isotope study on tiaojishan volcanic formation, Mujicun, north Taihang Mountain and implications for regional metallogeny and magmatism. *Acta Geol. Sin.* 90 (2), 250–266.

Duggen, S., Hoernle, K., Van, D. B. P., and Garbeschönberg, D. (2005). Post-collisional transition from subduction- to intraplate-type magmatism in the westernmost mediterranean: Evidence for continental-edge delamination of subcontinental lithosphere. *J. Petrology* 46 (6), 1155–1201. doi:10.1093/petrology/egi013

Fan, W. M. (1992). Destruction of aged lower lithosphere and accretion of asthenosphere mantle beneath eastern China. *Geotect. Metallogenia* 16, 171–180.

Foley, S. F., Barth, M. G., and Jenner, G. A. (2000). Rutile/melt partition coefficients for trace elements and an assessment of the influence of rutile on the trace element characteristics of subduction zone magmas. *Geochimica Cosmochimica Acta* 64 (5), 933–938. doi:10.1016/s0016-7037(99)00355-5

Gao, P., Zheng, Y. F., and Zhao, Z. F. (2016). Experimental melts from crustal rocks: A lithochemical constraint on granite petrogenesis. *Lithos* 266, 133–157. doi:10.1016/j.lithos.2016.10.005

Gao, S., Rudnick, R. L., Carlson, R. W., Mcdonough, W. F., and Liu, Y. S. (2002). Re–Os evidence for replacement of ancient mantle lithosphere beneath the North China craton. *Earth Planet. Sci. Lett.* 198 (3-4), 307–322. doi:10.1016/s0012-821x(02)00489-2

Gao, S., Rudnick, R. L., Yuan, H. L., Liu, X. M., Liu, Y. S., Xu, W. L., et al. (2004). Recycling lower continental crust in the North China craton. *Nature* 432 (7019), 892–897. doi:10.1038/nature03162

Gao, S., Zhang, J., Xu, W., and Liu, Y. (2009). Delamination and destruction of the North China craton. *Sci. Bull. (Beijing).* 54 (19), 3367–3378. doi:10.1007/s11434-009-0395-9

Gao, Y. F., Wei, R. H., Hou, Z. Q., Ma, G. X., Zhao, R. S., Chen, Z. K., et al. (2011). Mujicun porphyry copper mineralization: Response to mesozoic thinning of lithosphere in north China craton. *Mineral. Deposits* 30 (5), 890–902.

Gao, Y. F., Santosh, M., Hou, Z. Q., Wei, R. H., Ma, G. X., Chen, Z. K., et al. (2012). High Sr/Y magmas generated through crystal fractionation: Evidence from Mesozoic volcanic rocks in the northern Taihang orogen, North China Craton. *Gondwana Res.* 22 (1), 152–168. doi:10.1016/j.gr.2011.11.002

Geng, Y. S., Du, L. L., and Ren, L. D. (2012). Growth and reworking of the early precambrian continental crust in the North China craton: Constraints from zircon Hf isotopes. *Gondwana Res.* 21 (2-3), 517–529. doi:10.1016/j.gr.2011.07.006

Glazner, A. F., Bartley, J. M., Coleman, D. S., Gray, W., and Taylor, R. Z. (2004). Are plutons assembled over millions of years by amalgamation from small magma chambers? *GSA today* 14 (4/5), 4–12. doi:10.1130/1052-5173(2004)014<0004:apaomo>2.0.co;2

Goldfarb, R. J., and Santosh, M. (2014). The dilemma of the Jiaodong gold deposits: Are they unique? *Geosci. Front.* 5 (2), 139–153. doi:10.1016/j.gsf.2013.11.001

Griffin, W. L., Andi, Z., O'Reilly, S. Y., and Ryan, C. G. (1998). *Phanerozoic evolution of the lithosphere beneath the sino-Korean craton*. American Geophysical Union, 107–126.

Groves, D. I., and Santosh, M. (2016). The giant Jiaodong gold province: The key to a unified model for orogenic gold deposits? *Geosci. Front.* 7 (3), 409–417. doi:10.1016/j.gsf.2015.08.002

Hawkesworth, C. J., Cawood, P. A., Dhuime, B., and Kemp, T. I. (2017). Earth's continental lithosphere through time. *Annu. Rev. Earth Planet. Sci.* 45, 169–198. doi:10.1146/annurev-earth-063016-020525

Hawkesworth, C. J., Gallagher, K., Hergt, J. M., and McDermott, F. (1993). Mantle and slab contributions in arc magmas. *Annu. Rev. Earth Planet. Sci.* 21 (1), 175–204. doi:10.1146/annurev.ea.21.050193.001135

He, X. F., and Santosh, M. (2014). Crustal recycling through intraplate magmatism: Evidence from the Trans-North China orogen. *J. Asian Earth Sci.* 95, 147–163. doi:10.1016/j.jseaes.2014.02.011

He, X. F., Santosh, M., and Ganguly, S. (2017). Mesozoic felsic volcanic rocks from the North China craton: Intraplate magmatism associated with craton destruction. *Geol. Soc. Am. Bull.* 129 (7-8), 947–969. doi:10.1130/b31607.1

Hildreth, W., and Moorbath, S. (1988). Crustal contributions to arc magmatism in the Andes of Central Chile. *Contr. Mineral. Pet.* 98 (4), 455–489. doi:10.1007/bf00372365

Hou, Z. Q., Li, Q., Gao, Y., Lu, Y., Yang, Z., Wang, R., et al. (2015). Lower-crustal magmatic hornblendite in north China craton: Insight into the genesis of porphyry Cu deposits. *Econ. Geol.* 110 (7), 1879–1904. doi:10.2113/econgeo.110.7.1879

Houseman, G. A., Mckenzie, D. P., and Molnar, P. (1981). Convective instability of a thickened boundary layer and its relevance for the thermal evolution of continental convergent belts. *J. Geophys. Res.* 86 (B7), 6115–6132. doi:10.1029/jb086ib07p06115

Jiang, N., Liu, Y. S., Zhou, W. G., Yang, J. H., and Zhang, S. Q. (2007). Derivation of Mesozoic adakitic magmas from ancient lower crust in the North China craton. *Geochimica Cosmochimica Acta* 71 (10), 2591–2608. doi:10.1016/j.gca.2007.02.018

Lee, C. A., Luffi, P., and Chin, E. J. (2011). Building and destroying continental mantle. *Annu. Rev. Earth Planet. Sci.* 39, 59–90. doi:10.1146/annurev-earth-040610-133505

Li, N., Chen, Y., Santosh, M., and Pirajno, F. (2018). Late mesozoic granitoids in the qinling orogen, central China, and tectonic significance. *Earth-Science Rev.* 182 (182), 141–173. doi:10.1016/j.earscirev.2018.05.004

Li, Q., Santosh, M., and Li, S. R. (2013). Stable isotopes and noble gases in the xishimen gold deposit, central North China craton: Metallogeny associated with lithospheric thinning and crust-mantle interaction. *Int. Geol. Rev.* 55 (14), 1728–1743. doi:10.1080/00206814.2013.793445

Li, S. R., and Santosh, M. (2017). Geodynamics of heterogeneous gold mineralization in the North China Craton and its relationship to lithospheric destruction. *Gondwana Res.* 50, 267–292. doi:10.1016/j.gr.2017.05.007

Li, S. Z., Zhao, G., Dai, L., Liu, X., Zhou, L., Santosh, M., et al. (2012). Mesozoic basins in eastern China and their bearing on the deconstruction of the North China Craton. *J. Asian Earth Sci.* 47, 64–79. doi:10.1016/j.jseaes.2011.06.008

Li, X. Y., Li, S. Z., Huang, F., Wang, Y. M., Yu, S. Y., Cao, H. H., et al. (2019). Petrogenesis of high Ba–Sr plutons with high Sr/Y ratios in an intracontinental setting: Evidence from early cretaceous fushan monzonites, central North China craton. *Geol. Mag.* 156 (12), 1965–1981. doi:10.1017/s0016756819000256

Li, X. Y., Li, S. Z., Suo, Y. H., Somerville, I., Huang, F., Liu, X., et al. (2017). Early Cretaceous diabases, lamprophyres and andesites-dacites in Western Shandong, North China Craton: Implications for local delamination and Paleo-Pacific slab rollback. *J. Asian Earth Sci.* 160, 426–444. doi:10.1016/j.jseaes.2017.08.005

Li, X. Y., Zheng, J. P., Ma, Q., Xiong, Q., Griffin, W., and Lu, J. G. (2014). From enriched to depleted mantle: Evidence from cretaceous lamprophyres and paleogene basaltic rocks in eastern and central guangxi province, Western cathaysia block of south China. *Lithos* 184, 300–313. doi:10.1016/j.lithos.2013.10.039

Liu, A. K., Chen, B., Suzuki, K., and Liu, L. (2010). Petrogenesis of the mesozoic zijinguan mafic pluton from the Taihang mountains, north China craton: Petrological and Os–Nd–Sr isotopic constraints. *J. Asian Earth Sci.* 39 (4), 294–308. doi:10.1016/j.jseaes.2010.03.007

Liu, D. Y., Nutman, A. P., Compston, W., Wu, J. S., and Shen, Q. H. (1992). Remnants of≥ 3800 Ma crust in the Chinese part of the Sino-Korean craton. *Geol.* 20 (4), 339–342. doi:10.1130/0091-7613(1992)020<0339:romcit>2.3.co;2

Liu, D. Y., Page, R. W., Compston, W., and Wu, J. (1984). U-Pb zircon geochronology of late archaean metamorphic rocks in the taihangshan—wutaishan area, north China. *Precambrian Res.* 27 (1), 85–109. doi:10.1016/0301-9268(85)90007-5

Liu, J. G., Cai, R. H., Pearson, D. G., and Scott, J. M. (2019). Thinning and destruction of the lithospheric mantle root beneath the North China craton: A review. *Earth-Science Rev.* 196, 102873. doi:10.1016/j.earscirev.2019.05.017

Liu, L., Chen, B., and Liu, A. K. (2009). Petrogenesis of the Zijingguan mafic pluton, northern Taihang orogen: Constraints from petrology and geochemistry. *Earth Sci.* 34, 165–178.

Liu, S., Feng, C., Feng, G., Xu, M., Coulson, I. M., Guo, X., et al. (2017b). Timing, mantle source and origin of mafic dykes within the gravity anomaly belt of the Taihang-Da Hinggan gravity lineament, central North China Craton. *J. Geodyn.* 109, 41–58. doi:10.1016/j.jog.2017.05.006

Liu, S., Feng, C., Santosh, M., Feng, G., Coulson, I. M., Xu, M., et al. (2018). Integrated elemental and Sr-Nd-Pb-Hf isotopic studies of mesozoic mafic dykes from the eastern north China craton: Implications for the dramatic transformation of lithospheric mantle. *J. Geodyn.* 114, 19–40. doi:10.1016/j.jog.2017.11.007

Liu, X., Zhao, D. P., Li, S. Z., and Wei, W. (2017a). Age of the subducting Pacific slab beneath East Asia and its geodynamic implications. *Earth Planet. Sci. Lett.* 464, 166–174. doi:10.1016/j.epsl.2017.02.024

Ma, L., Jiang, S. Y., Hofmann, A. W., Dai, B. Z., Hou, M. L., Zhao, K. D., et al. (2014). Lithospheric and asthenospheric sources of lamprophyres in the Jiaodong Peninsula: A consequence of rapid lithospheric thinning beneath the North China craton? *Geochimica Cosmochimica Acta* 124 (1), 250–271. doi:10.1016/j.gca.2013.09.035

Ma, L., Jiang, S. Y., Hofmann, A. W., Xu, Y. G., Dai, B. Z., and Hou, M. L. (2016). Rapid lithospheric thinning of the North China Craton: New evidence from cretaceous mafic dikes in the Jiaodong Peninsula. *Chem. Geol.* 432, 1–15. doi:10.1016/j.chemgeo.2016.03.027

Ma, Q., and Xu, Y. (2021). Magmatic perspective on subduction of Paleo-Pacific plate and initiation of big mantle wedge in East Asia. *Earth-Science Rev.* 213, 103473. doi:10.1016/j.earscirev.2020.103473

Mao, J. W., Xie, G. Q., Zhang, Z. H., Li, X. F., Wang, Y. T., Zhang, C. Q., et al. (2005). Mesozoic large-scale metallogenic pulses in North China and corresponding geodynamic settings. *Acta Petrol. Sin.* 21 (1), 169–188.

Maruyama, S., Santosh, M., and Zhao, D. (2007). Superplume, supercontinent, and post-perovskite: Mantle dynamics and anti-plate tectonics on the Core–Mantle Boundary. *Gondwana Res.* 11 (1–2), 7–37. doi:10.1016/j.gr.2006.06.003

Mcdonough, W. F., and Sun, S. S., 1995. The composition of the Earth ☆. *Chem. Geol.*, 120(3-4): 223–253, doi:10.1016/0009-2541(94)00140-4

Mckenzie, D., and O'Nions, R. K. (1991). Partial melt distributions from inversion of rare earth element concentrations. *J. Petrology* 32 (5), 1021–1091. doi:10.1093/petrology/32.5.1021

Menzies, M., Xu, Y., Zhang, H., and Fan, W. (2007). Integration of geology, geophysics and geochemistry: A key to understanding the North China craton. *Lithos* 96 (1-2), 1–21. doi:10.1016/j.lithos.2006.09.008

Middlemost, E. A. K. (1994). Naming materials in the magma/igneous rock system. *Earth-Science Rev.* 37 (3-4), 215–224. doi:10.1016/0012-8252(94)90029-9

Morency, C., Doin, M. P., and Dumoulin, C. (2002). Convective destabilization of a thickened continental lithosphere. *Earth Planet. Sci. Lett.* 202 (2), 303–320. doi:10.1016/s0012-821x(02)00753-7

Niu, Y. L. (2005). Generation and evolution of basaltic magmas: Some basic concepts and a new view on the origin of mesozoic–cenozoic basaltic volcanism in eastern China. *Geol. J. China Univ.* 11 (1), 9–46.

Orozco-Garza, A., Dostal, J., Keppie, J. D., and Paz-Moreno, F. A. (2013). Mid-Tertiary (25-21 Ma) lamprophyres in NW Mexico derived from subduction-modified subcontinental lithospheric mantle in an extensional backarc environment following steepening of the Benioff zone. *Tectonophysics* 590, 59–71. doi:10.1016/j.tecto.2013.01.013

Pearce, J. A. (2008). Geochemical fingerprinting of oceanic basalts with applications to ophiolite classification and the search for Archean oceanic crust. *Lithos* 100 (1-4), 14–48. doi:10.1016/j.lithos.2007.06.016

Pearce, J. A., Harris, N. B. W., and Tindle, A. G. (1984). Trace element discrimination diagrams for the tectonic interpretation of granitic rocks. *J. Petrology* 25 (4), 956–983. doi:10.1093/petrology/25.4.956

Pearce, J. A., and Peate, D. W. (1995). Tectonic implications of the composition of volcanic arc magmas. *Annu. Rev. Earth Planet. Sci.* 23 (1), 251–285. doi:10.1146/annurev.ea.23.050195.001343

Peccerillo, A., and Taylor, S. R. (1975). Geochemistry of eocene calc-alkaline volcanic rocks from the Kastamonu area, Northern Turkey. *Contr. Mineral. Pet.* 58 (1), 63–81. doi:10.1007/bf00384745

Pitcher, W. S. (1997). *The nature and origin of granite*. Springer Science & Business Media.

Qu, K. (2012). *Geology and mineralization in Mujicun porphyry Cu-Mo deposit, northern Taihang Mt., China, master thesis*. Beijing), Beijing: China University of Geosciences.

Rapp, R. P., Shimizu, N., Norman, M. D., and Applegate, G. S. (1999). Reaction between slab-derived melts and peridotite in the mantle wedge: Experimental constraints at 3.8 GPa. *Chem. Geol.* 160 (4), 335–356. doi:10.1016/s0009-2541(99)00106-0

Rapp, R. P., and Watson, E. B. (1995). Dehydration melting of metabasalt at 8–32 kbar: Implications for continental growth and crust-mantle recycling. *J. Petrology* 36 (4), 891–931. doi:10.1093/petrology/36.4.891

Robinson, J. A. C., and Wood, B. J. (1998). The depth of the spinel to garnet transition at the peridotite solidus. *Earth Planet. Sci. Lett.* 164 (1-2), 277–284. doi:10.1016/s0012-821x(98)00213-1

Rudnick, R. L. (1995). Making continental crust. *Nature* 378 (6557), 571–578. doi:10.1038/378571a0

Santosh, M. (2010). Assembling North China Craton within the Columbia supercontinent: The role of double-sided subduction. *Precambrian Res.* 178 (1-4), 149–167. doi:10.1016/j.precamres.2010.02.003

Schmidt, A., Weyer, S., John, T., and Brey, G. P. (2009). HFSE systematics of rutile-bearing eclogites: New insights into subduction zone processes and implications for the Earth's HFSE budget. *Geochimica Cosmochimica Acta* 73 (2), 455–468. doi:10.1016/j.gca.2008.10.028

Shen, Z. C., Hou, Z. Q., Chen, Z. K., Li, Q. Y., Zhou, Y. M., and Wang, Z. M. (2015b). Molybdenite Re-Os isotopic dating and zircon SHRIMP U-Pb and Hf isotopic compositions of the Mujicun porphyry deposit. *Acta Petrologica Mineralogica* 4 (34), 526–538.

Shen, Z. C., Hou, Z. Q., Yu, F., Chen, Z. K., Li, Q. Y., Ma, G. X., et al. (2015a). SHRIMP zircon U-Pb ages and Hf isotopes of the intermediate-acidic rocks of

Wanganzhen complex in northern part of Taihang Mountains and their geological implications. *Acta Petrol. Sin.* 31 (5), 1409–1420.

Song, Y., Ding, H. Y., Qu, X. M., Wang, R. J., Zhou, W., and Wang, S. Z. (2014). Re–Os and U–Pb geochronology of the dawan Mo–Zn–Fe deposit in northern Taihang mountains, China. *Resour. Geol.* 64 (2), 117–135. doi:10.1111/rge.12032

Stern, C. R., and Kilian, R. (1996). Role of the subducted slab, mantle wedge and continental crust in the generation of adakites from the Andean Austral Volcanic Zone. *Contributions Mineralogy Petrology* 123 (3), 263–281. doi:10.1007/s004100050155

Sun, S. S., and Mcdonough, W. F. (1989). Chemical and isotopic systematics of oceanic basalts; implications for mantle composition and processes. *Geol. Soc. Lond. Spec. Publ.* 42 (1), 313–345. doi:10.1144/gsl.sp.1989.042.01.19

Tang, L., and Santosh, M. (2018). Neoarchean-paleoproterozoic terrane assembly and Wilson cycle in the North China craton: An overview from the central segment of the Trans-North China orogen. *Earth-Science Rev.* 182, 1–27. doi:10.1016/j.earscirev.2018.04.010

Tang, L., Santosh, M., and Teng, X. (2015). Paleoproterozoic (ca. 2.1–2.0 Ga) arc magmatism in the fuping complex: Implications for the tectonic evolution of the Trans-North China orogen. *Precambrian Res.* 268, 16–32. doi:10.1016/j.precamres.2015.07.001

Tang, L., Santosh, M., Tsunogae, T., and Teng, X. (2016). Late neoarchean arc magmatism and crustal growth associated with microblock amalgamation in the North China craton: Evidence from the fuping complex. *Lithos* 248, 324–338. doi:10.1016/j.lithos.2016.01.022

Tarney, J., and Jones, C. E. (1994). Trace element geochemistry of orogenic igneous rocks and crustal growth models. *J. Geol. Soc. Lond.* 151 (5), 855–868. doi:10.1144/gsjgs.151.5.0855

Walker, B. A., Jr, Miller, C. F., Claiborne, L. L., Wooden, J. L., and Miller, J. S. (2007). Geology and geochronology of the Spirit Mountain batholith, southern Nevada: Implications for timescales and physical processes of batholith construction. *J. Volcanol. Geotherm. Res.* 167 (1-4), 239–262. doi:10.1016/j.jvolgeores.2006.12.008

Wang, Q., Xu, J. F., Jian, P., Bao, Z. W., Zhao, Z. H., Li, C. F., et al. (2006). Petrogenesis of adakitic porphyries in an extensional tectonic setting, dexing, south China: Implications for the genesis of porphyry copper mineralization. *J. Petrology* 47 (1), 119–144. doi:10.1093/petrology/egi070

Wang, T., Guo, L., Zheng, Y., Donskaya, T., Gladkochub, D., Zeng, L., et al. (2012). Timing and processes of late Mesozoic mid-lower-crustal extension in continental NE Asia and implications for the tectonic setting of the destruction of the North China Craton: Mainly constrained by zircon U–Pb ages from metamorphic core complexes. *Lithos* 154, 315–345. doi:10.1016/j.lithos.2012.07.020

Wilde, S. A., Zhou, X., Nemchin, A. A., and Sun, M. (2003). Mesozoic crust-mantle interaction beneath the North China craton: A consequence of the dispersal of gondwanaland and accretion of Asia. *Geol.* 31 (9), 817–820. doi:10.1130/g19489.1

Wilson, M. (1993). Magmatic differentiation. *J. Geol. Soc. Lond.* 150 (4), 611–624. doi:10.1144/gsjgs.150.4.0611

Windley, B. F., Maruyama, S., and Xiao, W. J. (2010). Delamination/thinning of sub-continental lithospheric mantle under Eastern China: The role of water and multiple subduction. *Am. J. Sci.* 310 (10), 1250–1293. doi:10.2475/10.2010.03

Wu, F., Yang, J., Xu, Y., Wilde, S. A., and Walker, R. J. (2019). Destruction of the North China craton in the mesozoic. *Annu. Rev. Earth Planet. Sci.* 47 (1), 173–195. doi:10.1146/annurev-earth-053018-060342

Wu, F. Y., Lin, J. Q., Wilde, S. A., Zhang, X., and Yang, J. H. (2005). Nature and significance of the Early Cretaceous giant igneous event in eastern China. *Earth Planet. Sci. Lett.* 233 (1), 103–119. doi:10.1016/j.epsl.2005.02.019

Wu, F. Y., Liu, X. C., Ji, W. Q., Wang, J. M., and Yang, L. (2017). Highly fractionated granites: Recognition and research. *Sci. China Earth Sci.* 60 (7), 1201–1219. doi:10.1007/s11430-016-5139-1

Xu, W., Zhou, Q. J., Pei, F. P., Yang, D. B., Gao, S., Li, Q. L., et al. (2013). Destruction of the North China craton: Delamination or thermal/chemical erosion? Mineral chemistry and oxygen isotope insights from websterite xenoliths. *Gondwana Res.* 23 (1), 119–129. doi:10.1016/j.gr.2012.02.008

Xu, W., Zhu, D. C., Wang, Q., Weinberg, R. F., Wang, R., Li, S. M., et al. (2019). Constructing the early mesozoic gangdese crust in southern tibet by hornblende-dominated magmatic differentiation. *J. Petrology* 60 (3), 515–552. doi:10.1093/petrology/egz005

Xu, Y. G., Li, H. Y., Pang, C. J., and He, B. (2009). On the timing and duration of the destruction of the North China Craton. *Sci. Bull. (Beijing).* 54 (19), 3379–3396. doi:10.1007/s11434-009-0346-5

Xu, Y. G., Ma, J. L., Frey, F. A., Feigenson, M. D., and Liu, J. F. (2005). Role of lithosphere–asthenosphere interaction in the Genesis of Quaternary alkali and tholeiitic basalts from Datong, Western North China Craton. *Chem. Geol.* 224 (4), 247–271. doi:10.1016/j.chemgeo.2005.08.004

Xu, Y. G. (2001). Thermo-tectonic destruction of the archaean lithospheric keel beneath the Sino-Korean Craton in China: Evidence, timing and mechanism. *Phys. Chem. Earth Part A Solid Earth Geodesy* 26 (9-10), 747–757. doi:10.1016/s1464-1895(01)00124-7

Xue, F., Santosh, M., Kim, S. W., Tsunogae, T., and Yang, F. (2021). Thermo-mechanical destruction of archean cratonic roots: Insights from the mesozoic laiyuan granitoid complex, north China craton. *Lithos* 400, 106394. doi:10.1016/j.lithos.2021.106394

Xue, F., Santosh, M., Li, S., Zhang, J., and Tsunogae, T. (2019a). Early Cretaceous cryptoexplosive breccia-related gold mineralization in the North China Craton: Evidence from the Puziwan gold deposit. *Ore Geol. Rev.* 111, 102986. doi:10.1016/j.oregeorev.2019.102986

Xue, F., Santosh, M., Tsunogae, T., and Yang, F. (2019b). Geochemical and isotopic imprints of early cretaceous mafic and felsic dyke suites track lithosphere-asthenosphere interaction and craton destruction in the North China Craton. *Lithos* 326-327, 174–199. doi:10.1016/j.lithos.2018.12.013

Xue, F., Santosh, M., Tsunogae, T., Yang, F., and Zhou, H. (2020). The Genesis of high Ba-Sr adakitic rocks: Insights from an Early Cretaceous volcanic suite in the central North China Craton. *Geol. J.* 55 (7), 5398–5416. doi:10.1002/gj.3720

Yang, F., Santosh, M., Kim, S. W., Zhou, H., and Xue, F. (2019a). Early Cretaceous adakitic granitoids from the Zhijiazhuang skarn iron deposit, North Taihang Mountain, China: Implications for petrogenesis and metallogenesis associated with craton destruction. *Geol. J.* 54 (6), 3189–3211. doi:10.1002/gj.3320

Yang, F., Santosh, M., Kim, S. W., Zhou, H. Y., and Jeong, Y. J. (2020). Late mesozoic intraplate rhyolitic volcanism in the North China craton: Far-field effect of the westward subduction of the Paleo-Pacific plate. *GSA Bull.* 132, 291–309. doi:10.1130/b35123.1

Yang, F., Xue, F., Santosh, M., Wang, G., Kim, S. W., Shen, Z., et al. (2019b). Late mesozoic magmatism in the East qinling orogen, China and its tectonic implications. *Geosci. Front.* 10 (5), 1803–1821. doi:10.1016/j.gsf.2019.03.003

Yang, J., O'Reilly, S., Walker, R. J., Griffin, W., Wu, F. Y., Zhang, M., et al. (2010). Diachronous decratonization of the Sino-Korean craton: Geochemistry of mantle xenoliths from North Korea. *Geology* 38 (9), 799–802. doi:10.1130/g30944.1

Yang, J. (1991). The geochemical features and their Genesis of lamprophyres in Laiyuan-Fuping area, Hebei Province, China. *Geoscience* 3 (5), 330–337.

Yang, J. (1989). The petrological studies on lamprophyres in laiyuan and fuping area, Hebei. *Acta Petrologica Mineralogica* (8), 12–24.

Zak, J., and Paterson, S. R. (2005). Characteristics of internal contacts in the Tuolumne Batholith, central Sierra Nevada, California (USA): Implications for episodic emplacement and physical processes in a continental arc magma chamber. *Geol. Soc. Am. Bull.* 117 (9-10), 1242–1255. doi:10.1130/b25558.1

Zhai, M. G., and Santosh, M. (2011). The early precambrian odyssey of the North China craton: A synoptic overview. *Gondwana Res.* 20 (1), 6–25. doi:10.1016/j.gr.2011.02.005

Zhai, Y. Y., Xie, J. C., and Dong, G. C. (2014). The genetic significance of amphiboles from the ultramafic rocks of Wang'anzhen batholith in northern Taihang Mountains. *Acta Petrologica Mineralogica* 33 (2), 273–282. doi:10.3969/j.issn.1000-6524.2014.02.006

Zhang, C., Li, C., Deng, H., Liu, Y., Liu, L., Wei, B., et al. (2011). Mesozoic contraction deformation in the Yanshan and northern Taihang mountains and its implications to the destruction of the North China Craton. *Sci. China Earth Sci.* 54 (6), 798–822. doi:10.1007/s11430-011-4180-7

Zhang, H. D., Liu, J. C., Wang, J. Y., Zhang, S. N., Hu, B., Wang, D. Q., et al. (2016). Petrology, geochronology and geochemistry characteristics of Wang'anzhen complex in the northern Taihang Mountain and their geological significance. *Acta Petrol. Sin.* 32 (3), 727–745.

Zhang, H. D., Liu, J., Santosh, M., Tao, N., Zhou, Q., and Hu, B. (2017). Ultra-depleted peridotite xenoliths in the Northern Taihang mountains: Implications for the nature of the lithospheric mantle beneath the North China craton. *Gondwana Res.* 48, 72–85. doi:10.1016/j.gr.2017.04.009

Zhang, H., Sun, M., Zhou, X. H., Fan, W. M., Zhai, M. G., and Yin, J. F. (2002). Mesozoic lithosphere destruction beneath the North China craton: Evidence from major-trace-element and Sr–Nd–Pb isotope studies of fangcheng basalts. *Contrib. Mineral. Pet.* 144 (2), 241–254. doi:10.1007/s00410-002-0395-0

Zhang, J., Li, S., Santosh, M., Wang, J., and Li, Q. (2015). Mineral chemistry of high-Mg diorites and skarn in the Han-Xing Iron deposits of South Taihang Mountains, China: Constraints on mineralization process. *Ore Geol. Rev.* 64, 200–214. doi:10.1016/j.oregeorev.2014.07.007

Zhang, S. H., Zhao, Y., Davis, G. A., Ye, H., and Wu, F. (2014). Temporal and spatial variations of Mesozoic magmatism and deformation in the North China

Craton: Implications for lithospheric thinning and decratonization. *Earth-Science Rev.* 131 (4), 49–87. doi:10.1016/j.earscirev.2013.12.004

Zhang, S. N. (2014). *Geochemical characteristics and genetic mechanism of wanganzhen complex in Taihang Mountains*. Beijing), Beijing: China University of Geosciences.

Zhang, Y., Chen, B., Shao, J. A., and Zhai, M. G. (2003). Geochemistry and origin of late mesozoic lamprophyre dykes in Taihang mountains, north China. *Acta Petrologica Mineralogica* 22 (1), 29–33. doi:10.3969/j.issn.1000-6524.2003.01.004

Zhao, G. C., Cawood, P. A., Li, S., Wilde, S. A., Sun, M., Zhang, J., et al. (2012). Amalgamation of the North China craton: Key issues and discussion. *Precambrian Res.* 222, 55–76. doi:10.1016/j.precamres.2012.09.016

Zhao, G. C., Sun, M., Wilde, S. A., and Li, S. Z. (2005). Late archean to paleoproterozoic evolution of the North China craton: Key issues revisited. *Precambrian Res.* 136 (2), 177–202. doi:10.1016/j.precamres.2004.10.002

Zheng, J. P., O'Reilly, S. Y., Griffin, W., Lu, F., Zhang, M., and Pearson, N. (2001). Relict refractory mantle beneath the eastern north China block: Significance for lithosphere evolution. *Lithos* 57 (1), 43–66. doi:10.1016/s0024-4937(00)00073-6

Zheng, T. Y., Chen, L., Zhao, L., and Zhu, R. X. (2007). Crustal structure across the Yanshan belt at the northern margin of the North China Craton. *Phys. Earth Planet. Interiors* 161 (1), 36–49. doi:10.1016/j.pepi.2007.01.004

Zheng, Y. F., Xu, Z., Zhao, Z. F., and Dai, L. Q. (2018). Mesozoic mafic magmatism in North China: Implications for thinning and destruction of cratonic lithosphere. *Sci. China Earth Sci.* 61 (4), 353–385. doi:10.1007/s11430-017-9160-3

Zhu, G., Chen, Y., Jiang, D., and Lin, S. (2015). Rapid change from compression to extension in the North China craton during the early cretaceous: Evidence from the yunmengshan metamorphic core complex. *Tectonophysics* 656, 91–110. doi:10.1016/j.tecto.2015.06.009

Zhu, R. X., Chen, L., Wu, F. Y., and Liu, J. L. (2011). Timing, scale and mechanism of the destruction of the North China Craton. *Sci. China Earth Sci.* 54 (6), 789–797. doi:10.1007/s11430-011-4203-4

Zhu, R. X., and Xu, Y. G. (2019). The subduction of the west Pacific plate and the destruction of the North China Craton. *Sci. China Earth Sci.* 62, 1340–1350. doi:10.1007/s11430-018-9356-y

Zhu, R. X., Yang, J., and Wu, F. Y. (2012). Timing of destruction of the North China craton. *Lithos* 149, 51–60. doi:10.1016/j.lithos.2012.05.013